Lateral buckling of submarine pipelines under high temperature and high pressure - A literature review

Jie Cai, Philippe Le Grognec

Lateral buckling of submarine pipelines under high temperature and high pressure - a literature review

Jie Cai[a,b], Philippe Le Grognec[a,*]

[a]*ENSTA Bretagne, UMR CNRS 6027, IRDL, F-29200 Brest, France*
[b]*SDU Engineering Operations Management, Department of Technology and Innovation, University of Southern Denmark, Odense, Denmark*

Abstract

This paper consists of a literature review on the latest research progress about the lateral buckling of submarine pipelines under high temperature (HT) and high pressure (HP). First, the main general assumptions and simplifications made in the context of pipe lateral buckling are summarized in order to better understand the practical behavior of submarine pipelines. The governing equations of pipelines under uniaxial compression are then derived. Next, the controversial but widely deployed concept of effective axial force under complex sea environment is introduced. Influential parameters including initial imperfections, pipe-seabed interactions and residual stresses are elaborated and discussed. Furthermore, numerical simulation methods and experimental tests dealing with the lateral buckling of pipelines are presented as well. Controlled methods which are practically used for buckle initiation are described. This paper also reveals the remaining challenges and new tendencies, such as the use of data-driven methods for the smart prediction of pipe buckling. Finally, a specific case study is numerically conducted. It is found that the effect of axial friction variation can be generally ignored in practical calculations. This paper may provide a guidance for the design and research on pipelines in the future.

Keywords: Submarine pipelines, Lateral buckling, Literature review, Effective axial force, HT/HP

Nomenclature

α	Thermal expansion coefficient
μ_A	Axial friction coefficient
μ_L	Lateral friction coefficient
ω_{max}	Supreme natural frequency

*Corresponding author.
Email address: philippe.le_grognec@ensta-bretagne.fr (Philippe Le Grognec)

ρ_{max} Maximum curvature radius

σ_r Residual stress

σ_y Yield stress

A Cross-section area of the pipe

A_e Cross-sectional area of external pipe

A_i Cross-sectional area of internal pipe

E Young's modulus

H_{berm} Berm resistance

I Second moment of area of the cross-section

k_s Lateral stiffness of the spring distribution

L (Half) buckling length

L_0 (Half) wavelength of imperfection

l_s Slip length

M Bending moment

N True wall force

P Effective axial force

P_{cr} Critical buckling load

q Self-weight per unit length of the pipeline

t_{plough} Plough depth

u Longitudinal displacement

u_φ Axial movement at full mobilization

u_s Resultant longitudinal movement at buckle/slip length interface

V_{ac} Strain energy due to axial compression

V_{pb} Strain energy due to pure bending

w Lateral deflection

w_0 Lateral deflection of imperfection

w_m Maximum buckling amplitude

w_{0m} Maximum amplitude of imperfection

1. Introduction

With the growing exploitation of oil and gas into deep and even ultra-deep water, the design of submarine pipelines currently faces big challenges (Jayson et al., 2008; Cai et al., 2017). For instance, in deep water, the internal pressure in submarine pipelines can reach up to 10 MPa and the temperature can be higher than 100^oC (Taylor and Gan, 1986; Karampour et al., 2013a). Moreover, the internal pressure may attain 44.8 MPa for a pipeline in ultra-deep water, whereas the operation temperature may be 177^oC (Jukes et al., 2009). Under such extreme conditions of HT/HP, pipelines on the seabed tend to move so as to dissipate accumulated strain energy. High temperature and high pressure variations induce compressive axial loads in pipelines whose boundaries are constrained or partially constrained (an experimental test has been specifically elaborated in order to demonstrate this special phenomenon (Palmer et al., 1974)). As a consequence of such uniaxial compression, upheaval and/or lateral buckling are likely to occur in submarine pipelines, as seen in Figure 1. Inevitably, the structural integrity of these pipelines will be affected. Therefore, one of the big challenges nowadays in submarine pipeline industry is the buckling phenomenon resulting from the high temperatures and high pressures encountered. Both internal and external mechanisms associated with this phenomenon should be clarified so that catastrophic damage of pipelines can be effectively avoided in engineering practice.

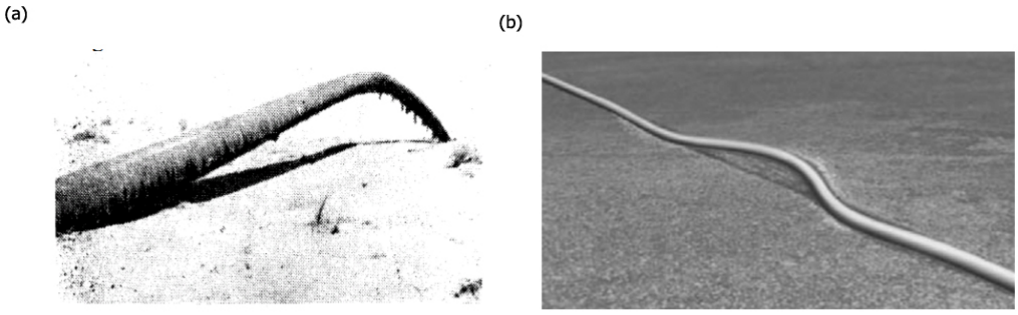

Figure 1: Upheaval buckling (a) and lateral buckling (b) of a pipeline (Liu, 2013)

Note that the buckling phenomenon can be viewed here as a structural response to a high compressive axial force, but not as a real failure mode. However, the occurrence of buckling in pipelines always results in severe consequences. As elaborated in DNV-RP-F110 for the global buckling of submarine pipelines (DNV, 2018), the failure modes of pipelines subsequent to buckling include fracture, fatigue and excessive displacement. The sudden appearance of buckling may lead to a loss of containment (Pasqualino et al., 2001; White and Cheuk, 2008). Some real accidents of submarine pipelines recorded in the past decades were due to the occurrence of lateral buckling, which produced severe damages on structures and then a huge loss of assets. One serious accident, involving upheaval buckling, occurred during the construction of a 36-inch pipeline in Colombia, as reported by Palmer et al. (1999). In January 2000 in the Guanabara Bay of Brazil, a leaking pipeline has released 1.3 million liters of oil due to lateral buckling, which eventually caused a local failure and the rupture of the pipe walls. This catastrophic accident had naturally a very damaging effect on marine life in the ocean (da Costa et al., 2002). Another documented

accident of pipeline happened in the Erskine field of the North Sea (McKinnon et al., 2001). It led to an 11-month shutdown of the entire project.

In the past decades, a considerable amount of research on the buckling of pipelines has been conducted. In the late 1960s, Allan (1968) designed an experimental test on the upheaval buckling of an axially compressed strip. Later on, Kerr (1978) studied the upheaval buckling of track foundations on the basis of the observation of railway tracks. Hobbs (1984) applied the same method in the context of pipelines and summarized analytical solutions in terms of buckling force and buckling amplitude. His analytical solutions for five different buckling modes (to be known as Mode 1 to Mode 5), displayed in Figure 2, are since then widely adopted by researchers. No initial imperfection was accounted for. Based on this study, Taylor and Gan (1986) analytically investigated the lateral buckling of submarine pipelines accounting for initial imperfections and deformation-dependent axial friction resistance. Imperfections in terms of Mode 1 and Mode 2 were adopted. More recently, Karampour et al. (2013a) studied the effects of these different types of initial imperfections both analytically and numerically. Specific parameters pertaining to initial imperfections such as amplitudes and half-wavelengths were investigated. Hong et al. (2015b) analytically studied the lateral buckling of pipelines with an initial imperfection in the shape of Mode 3, adopting the same derivation method as in Taylor and Gan (1986). Despite the fact that Mode 1 (symmetric) was first proposed for upheaval buckling, for which the equilibrium condition requires concentrated lateral forces at each end of the buckle, the lateral buckling mode of pipelines is rather prone to identify to Mode 3, in absence of such concentrated forces. Using initial imperfections of Mode 3 type, Karampour (2018) further investigated the effect of closely spaced imperfections on a pipeline laid on even seabed. Other research related to the buckling of submarine pipelines can also be found in Maltby and Calladine (1995b), Miles and Calladine (1999), Cheuk et al. (2007), Jukes et al. (2009) and Zhang et al. (2019), among others.

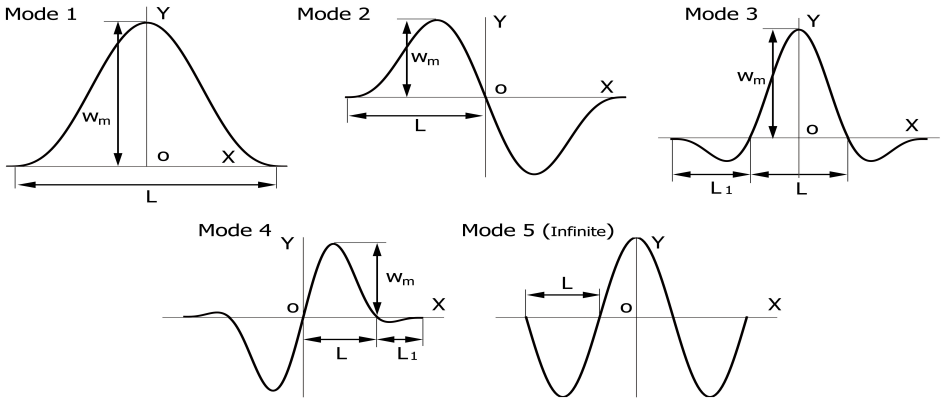

Figure 2: Five typical buckling shapes in pipelines (based on the definition of Hobbs (1984))

The vast majority of previous research focused on the uncontrolled (or unplanned) buckling of submarine pipelines. Solutions in terms of critical buckling forces, maximum buckle amplitudes or maximum bending moments were proposed under some particular conditions. As already mentioned, this sudden buckling without control will certainly affect the integrity and safety of the

pipelines. Conversely, the utilization of these solutions in order to control lateral buckling is meaningful in practice (Perinet et al., 2011). As a result, the investigation of controlled lateral buckling of submarine pipelines is crucial and various methods have emerged in recent years (Hoor et al., 2014).

Generally, there are two types of methods for such control. The traditional method is merely to restrain the movement of pipelines subjected to HT/HP on the seabed, whereas the modern method is to allow (even favour) the formation of global buckles in a controlled manner so that the strains, due to thermal expansion for instance, can be released safely. The former way includes trenching (Wang et al., 2018c), burying (Bai and Bai, 2014b) and rock-dumping (White and Cheuk, 2008) on the seabed, which have been demonstrated to be effective. However, these methods are far too expensive to be deployed in reality, especially with extra deep depth and complex sea environment. In order to figure out this drawback, the planned lateral buckling has been proposed and is still widely used nowadays, as it produces more benign buckles than uncontrolled methods (Liu et al., 2014; Zhang et al., 2018b; Chee et al., 2018; Zhang et al., 2019). Specific engineering measures, such as the use of snake-lays, sleepers, local weight reductions, or the distributed buoyancy technique, are employed to promote a reliable formation of lateral buckles at planned locations (Harrison et al., 2003; Peek and Yun, 2007; Urthaler et al., 2012; Shi and Wang, 2014). In this way, the lateral buckling can be well controlled in terms of buckle spaces and operating loads. In ultra-deep water, the design of submarine pipelines faces, however, many more challenges than usual (Jukes et al., 2009). Conventional single-walled pipelines are not suitable anymore (Zhang et al., 2018a). Hence, new types of pipelines were proposed such as the Pipe-in-Pipe (PIP) pipeline. Likewise, the buckling behavior of such pipelines is needed to be investigated.

This paper will majorly focus on the current submarine pipelines made of metallic materials. Composite or other novel types of pipelines will not be included, barring exceptional cases. The upheaval buckling of submarine pipelines will not be discussed in detail as well. Instead, one will just concentrate on the lateral buckling phenomenon and its relevant parameters. Furthermore, this paper will only focus on the global buckling of pipelines. The subsequent structural failure modes such as fracture and fatigue will not be discussed extensively.

The objective of this paper is to present the latest research progress on the lateral buckling of submarine pipelines under HT/HP based on a literature review. Some of the new challenges concerning lateral buckling of pipelines are finally revealed, so as to provide guidance for the future design and research in this field. Advanced techniques such as data-driven methods are briefly discussed in order to have a smart prediction of pipeline buckling in the future. The paper is organized as follows. In Section 2, the general simplifications classically achieved for the investigation of lateral buckling of pipelines are recalled, concerning the internal/external pressure, the pipe beam theory and the seabed consideration. These assumptions will be the basis of following discussions. In Section 3, the standard governing equations of the lateral buckling of pipelines on the seabed are derived. The corresponding solutions are displayed and discussed. In Section 4, the concept of effective axial force due to the variation of HT/HP is clarified. From Sections 5 to 7, several influential parameters on lateral buckling of submarine pipelines are analyzed, including initial imperfections, pipe-seabed interactions and residual stresses. The control methods allowing to initiate selectively the lateral buckling of pipelines are also summarized in Section 8. Accounting for all these factors, numerical methods are then discussed in Section 9 for the purpose

of lateral buckling simulation. In Section 10, experimental works on the buckling of pipelines are outlined, which provide reference results for theoretical/numerical validation. In Section 11, the procedure of building an empirical method for pipe buckling predictions is proposed, combining the results from both numerical computations and experimental tests. The data-driven methods are discussed. A final case study of a pipeline with imperfections subjected to uniaxial compression is handled in Section 12, where the effects of the variation of axial friction resistance are specifically investigated. Finally, the paper ends with some concluding remarks.

2. General simplifications related to lateral buckling

Assumptions and simplifications are classically made throughout the derivation of the governing equations of lateral buckling of pipelines, in order to facilitate the analytical or even numerical resolution of such equations. Because of such hypotheses, there is a real risk to ignore some actually crucial physical phenomena. Hence, there is a necessity to clarify and highlight these simplifications. In this section, the most common assumptions are listed, concerning the internal and external pressures, the pipe-beam theory and the seabed representation, respectively. These aspects will be discussed in more details in the following sections.

2.1. Internal/external pressure

Thermal expansion is the main cause of uniaxial compression in pipelines. However, the influence of internal/external pressure on the global buckling of pipelines cannot be ignored. Hence, the concept of effective axial force has been proposed so as to take into account these pressure effects in a simplified way. In short, the effect of pipe pressures may be converted into an equivalent axial force, and eventually into a temperature variation for practical application (Palmer et al., 1974; Fyrileiv and Collberg, 2005; Fyrileiv et al., 2013). The lateral buckling analysis of submarine pipelines can then be largely simplified. Elaborations on how to properly consider these pressure effects are given in Section 4.

2.2. Pipe-beam model

Another important simplification concerns the pipe representation in modeling approaches. The length of submarine pipelines normally extends to hundreds of kilometers, which is much larger than the pipe diameter and thickness. The elastic Euler-Bernoulli beam theory (Timoshenko and Gere, 2009) is therefore adopted for the investigation of lateral buckling of pipelines with such large slenderness. In many works (Hobbs, 1984; Taylor and Gan, 1986; Ju and Kyriakides, 1988; Taylor and Tran, 1993; Karampour et al., 2013a; Hong et al., 2015b), the pipes are defined as beams resting on a rigid seabed without any penetration. Under such a simplification, the torsional effects are generally assumed to be small and thus ignored (Zhu et al., 2015; Liu and Wang, 2018). Note that such hypotheses are not always satisfied. For instance, the current authors have investigated the torsional effects on pipe lateral buckling, and they analytically demonstrated a significant influence of torsion under some specific boundary conditions (Le Grognec et al., 2020). As another simplification, the principle of superposition, which allows one to account efficiently for the cumulative effects of different loads on the structural response, is typically applied once the interactions between each individual load can be neglected. A common criterion for the use of this principle is that the lateral buckling slope of the pipeline is not larger than 0.1 *rad*.

2.3. Seabed interaction

The pipe-seabed interaction is another important factor affecting the buckling behavior. When a pipeline is resting on the seabed, the practical transverse loads acting on the pipeline during lateral buckling vary according to the type of seabed. The types of seabed generally investigated in the literature are soft clay (Verley and Lund, 1995; Cheuk and Bolton, 2006; Bruton et al., 2006; Cheuk et al., 2007; Oliveira et al., 2010), stiff clay (White and Cheuk, 2008) and sand (Zhang et al., 2019). When resting on soft clay or sand, a pipe is susceptible to penetrate into the seabed to a finite depth, fashioning thus a finite contact area on the pipe bottom.

A conventional design practice for pipes on the seabed is to identify the pipe-seabed interaction to a frictional contact, with friction forces proportional to the pipe effective weight underwater (q) regardless of the vertical load variations. In fact, the actual uneven seabed is supposed to be flat without extra disturbances, and it is normally assumed that the lateral friction is fully mobilized everywhere (Kerr, 1978). Alternatively, the pipe-seabed interaction can be more simply represented using a spring distribution with a given stiffness linear density k_s (in N/m^2) (Miles and Calladine, 1999; Galgoul et al., 2004; Zhang and Duan, 2015; Zhang et al., 2019). Detailed explanations on pipe-seabed interaction models will be provided in Section 6.

3. Theoretical analysis of pipe lateral buckling

This section is dedicated to present the stability analysis of a submarine pipeline from a theoretical point of view. More precisely, the governing equations of a pipe subjected to longitudinal compression are derived, allowing for the prediction and analysis of lateral buckling. Classical solutions are recalled and discussed. For simplicity purposes, an idealized submarine pipeline is first considered, without initial imperfections, laying on a rigid even seabed. The interaction between the pipe and the seabed is characterized by dry Coulomb friction. The Euler-Bernoulli beam theory (Timoshenko and Gere, 2009) is adopted, in the framework of linear elasticity.

Before deriving the governing equations, an important factor that should be clarified concerns the virtual anchor point. The effective pipe length to be investigated and the practical boundary conditions will be identified upon this clarification. Throughout the study, simply-supported or built-in boundary conditions may be intuitively enforced at the ends of the considered beam-like structure laying on the seabed. However, the ends of an overall pipeline are free to expand in practice. As seen in Figure 3, the pipe ends can generally expand freely (to some extent) through low-friction mechanical sliders, named Pipeline End Manifolds (PLEM) (Jayson et al., 2008; Van den Abeele et al., 2015; Chee et al., 2018; Konuk, 2018). Under these circumstances, the effective axial force at pipe ends without constraints is equal to zero. Owing to axial frictional resistance from the seabed, an effective axial compressive force may increase yet along the pipeline during the process of thermal expansion, leading to buckling. If the pipeline is long enough, there is one (or rather several) limit position along the pipeline route, from where the pipeline does not move axially towards a buckle or the pipeline end. These locations have been defined in DNV (2018) and are called virtual anchor points. In the anchor zones (where the pipe does not move axially), axial strains are null (there is no axial expansion) and the axial friction force equals the expansion force of the pipeline (namely the effective axial force). Figure 4 represents a scheme of a pipeline

experiencing lateral buckling and the corresponding axial load distribution. If the pipeline is sufficiently long, such localized buckles may form. Each buckle lies within its own virtual anchor space, as depicted by segment AOD in Figure 4. Points A and D stand for the virtual anchor points, while BOC is the lateral buckled region of the pipeline and L_s corresponds to the slip-length. With the occurrence of a buckle, the axial force within the buckled region decreases, associated with an increasing axial expansion (or feed-in) of the pipeline due to the bending deformation and the corresponding release of stored energy. One can therefore distinguish between the (critical) axial compressive force P_0 in the anchor zone and the reduced axial force within the buckled region P, which is classically assumed to be uniform. Between the anchor zones and the buckled regions (within segments AB and CD in Figure 4), the axial force switches between these two values and the pipe may slip, so that longitudinal boundary conditions (zero axial displacements and strains during buckling) must be consistently applied at the anchor points.

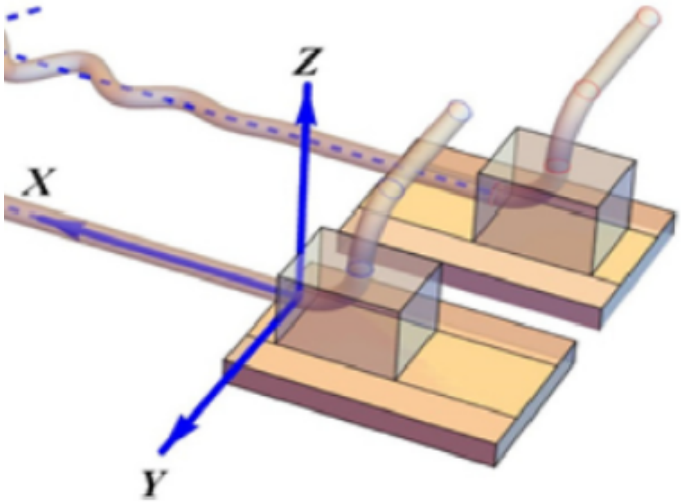

Figure 3: Representation of a long straight pipeline ending at a sliding PLEM during operation (Konuk, 2018)

In light of all these factors, the length of a pipeline during lateral buckling analysis can be either simply selected as the length of a given localized buckle between two virtual anchor points, or as the entire pipe length including multiple buckles. In this section, only a short pipe segment is considered with a unique buckle. Simply-supported boundary conditions are assumed at the ends of the buckled region, that is, the transverse displacement and the bending moment are both equal to zero.

3.1. Preliminary review of theoretical works on the lateral buckling of pipelines

Energy methods such as the principle of virtual work are the most widely used approaches in the literature for deriving the governing equations of pipeline buckling (Timoshenko and Gere, 2009; Bažant, 2000; McCarron, 2018). More specifically, Rayleigh-Ritz and Galerkin methods are among the most common solution procedures involving these energy methods used for the purpose of stability analyses (Chen and Lui, 1987).

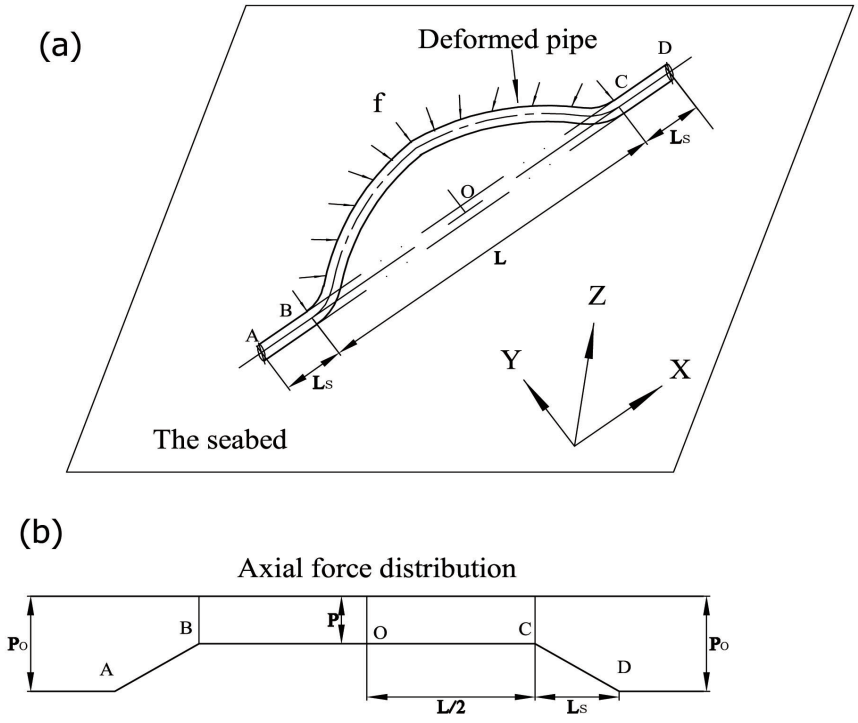

Figure 4: Lateral buckling of a long pipeline: (a) occurrence of a buckle between virtual anchor points; (b) axial force distribution around the buckled zone

Based on the virtual work principle, Timoshenko and Gere (2009) derived first a mathematical solution for the buckling capacity of a perfect straight beam supported by an elastic foundation, providing the corresponding buckling length L. The foundation was defined by a uniform lateral stiffness distribution. Kerr (1978) also used the principle of virtual work and analytically studied the buckling response of similar structures, introducing four typical buckling modes based on the observation of railway tracks. Upper-bound estimates of the critical buckling loads were obtained by the use of Galerkin method. Hobbs (1984) generalized these analytical solutions so as to cover the case of offshore pipelines, and also investigated the pre-buckling and post-buckling behaviors of pipelines. A new buckling mode (Mode 5) was added in the analysis, taking the form of an infinite sine wave (see Figure 2). In both previous analyses, the influence of initial imperfections was not accounted for. The only difference between them lies in the definition of buckling length. For instance, Hobbs (1984) defined the buckling length of Mode 3 as the width of the center lobe, whereas Kerr (1978) identified the same length to the half-width of the entire buckled shape. In the present paper, for clarity purposes, the definition of the buckling length L will be always based on Hobbs (1984). Later, Taylor and Gan (1986) analytically investigated the buckling of submarine pipelines accounting for initial imperfections. They were assumed to take the form of the aforementioned buckling modes. On another issue, Chen and Lui (1987) and Bažant (2000) performed the lateral buckling analysis of a pipeline, accounting for an elastic-plastic soil resistance. The Rayleigh-Ritz method was used, by means of a specific application of the principle of stationary potential energy in this non-conservative framework. Finally, let us cite Karampour et al. (2013a), who thoroughly investigated the lateral buckling of pipelines from an analytical point of view. A geometric imperfection was also introduced, but here in the form of a simple sine half-wave with the half-wavelength equal to the total length of the pipe.

3.2. Derivation of governing equations

The governing equations of a perfect submarine pipeline under uniaxial compression are derived in this section, using energy methods. Based on Euler beam theory, the kinematics is defined by two displacement fields, namely the longitudinal displacement u (along x-axis) and the lateral displacement w of the pipeline. The torsional effects and the influence of shear forces are not accounted for in the following derivation. It is assumed that the pipe buckles in Mode 1 with a buckling length L, as seen in Figure 4. Moreover, the variation of axial force within the buckle is not accounted for, so that a constant force P is assumed. Only half of the pipe is considered due to symmetry.

At this point, the entire strain energy of the pipeline V consists of the strain energy due to pure bending V_{pb} and the strain energy due to axial compression V_{ac}:

$$\begin{aligned} V &= V_{pb} + V_{ac} \\ &= \frac{1}{2} EI \int_{-L/2}^{L/2} \left(\frac{\partial^2 w}{\partial x^2} \right)^2 dx + \frac{1}{2} EA \int_{-L/2}^{L/2} \left(\frac{\partial u}{\partial x} \right)^2 dx \end{aligned} \tag{1}$$

Then, one has to express the overall work due to external loads. Owing to the former simplifications, there remain only two basic external loads on subsea pipelines: the effective axial force

P and the lateral soil resistance. Concerning the soil resistance, it is supposed that there is no embedment of the pipe into the soil due to the assumption of a rigid seabed. Thus, for simplification purposes, the lateral force can be assumed to be exerted through a spring distribution with a lateral stiffness by unit length of k_s, which can be expressed as the submerged pipe effective weight.

The work due to the effective axial force is related to the axial shortening of the pipe, but mostly to the flexural shortening ΔL of the pipeline due to bending, that is the difference between its original length and the horizontal projection of the bent shape (Young et al., 2002):

$$\Delta L = \frac{1}{2}\int_{-L/2}^{L/2}\left(\frac{\partial w}{\partial x}\right)^2 dx \tag{2}$$

Hence, the overall work W due to external loads can be written as the sum of the work due to axial shortening W_{axial}, the work due to flexural shortening $W_{flexural}$ and the work due to soil resistance W_{soil}:

$$\begin{aligned} W &= W_{axial} + W_{flexural} + W_{soil} \\ &= \frac{1}{2}P\int_{-L/2}^{L/2}\frac{P}{EA}dx + \frac{1}{2}P\int_{-L/2}^{L/2}\left(\frac{\partial w}{\partial x}\right)^2 dx - \frac{1}{2}\int_{-L/2}^{L/2}k_s w^2 dx \end{aligned} \tag{3}$$

Therefore, the total potential energy Π of the pipeline within a buckle can be written as the summation of the overall strain energy V and the force function $U = -W$:

$$\begin{aligned} \Pi &= U + V \\ &= \frac{1}{2}\int_{-L/2}^{L/2}\left[EI\left(\frac{\partial^2 w}{\partial x^2}\right)^2 - P\left(\frac{\partial w}{\partial x}\right)^2 + EA\left(\frac{\partial u}{\partial x}\right)^2 - \frac{P^2}{EA} + k_s w^2\right]dx \\ &= \int_{-L/2}^{L/2} F\left(x, u, \frac{\partial u}{\partial x}, w, \frac{\partial w}{\partial x}, \frac{\partial^2 w}{\partial x^2}\right)dx \end{aligned} \tag{4}$$

As seen in Equation (4), the total potential energy is an integral functional depending on both axial and lateral displacement fields and their derivatives. Based on the principle of stationary potential energy, the first-order variation of Π should be zero when the pipe is in equilibrium, which can be expressed as follows:

$$\delta\Pi = \frac{\partial \Pi}{\partial u_d}\delta u_d = 0 \qquad \forall \delta u_d \text{ kinematically admissible} \tag{5}$$

where u_d is the displacement vector and δu_d a corresponding virtual displacement field. Substituting expression (4) into the variational equation (5) gives rise to a new integral equation in terms of functional F. After integration by parts, it leads to the classical Euler's equations, which can be written in a generic way as follows:

$$F_{,u_d} - \frac{d}{dx}F_{,u_d'} + \frac{d^2}{dx^2}F_{,u_d''} = 0 \tag{6}$$

where $F_{,u_d}$ denotes the derivative of F with respect to u_d and so on.

By replacing u_d in Equation (6) by u and w successively, one obtains the two following differential equations governing the pipe response under uniaxial compression with lateral force:

$$EA\frac{\partial^2 u}{\partial x^2} = 0 \qquad -L/2 \leq x \leq L/2 \tag{7}$$

$$EI\frac{\partial^4 w}{\partial x^4} + P\frac{\partial^2 w}{\partial x^2} + k_s w = 0 \qquad -L/2 \leq x \leq L/2 \tag{8}$$

The two governing equations above are independent of each other since the coupling effects between axial and lateral displacements are not accounted for. Therefore, in most practical situations of lateral buckling of submarine pipelines, only Equation (8) has to be solved.

In the slip-length of the pipeline, outside the buckle, there is no lateral deflection, but an extra equilibrium equation should be satisfied, related to the longitudinal displacement:

$$EA\frac{\partial^2 u}{\partial x^2} = -\mu_A q \qquad L/2 \leq x \leq L/2 + L_s \text{ and } -L_s - L/2 \leq x \leq -L/2 \tag{9}$$

involving the pipe-soil axial friction coefficient μ_A and the submerged pipe effective weight q.

3.3. Analytical solutions of lateral buckling

So far, the governing equations of pipelines under uniaxial compression have been derived. In what follows, some details are given for solving these equations under practical boundary conditions. Typical solutions from literature are also presented and discussed.

3.3.1. Direct solutions

The governing equations in hand are found to be high-order Ordinary Differential Equations (ODEs). Direct solutions can thus be naturally sought by directly solving these complex equations. A general solution in the form of trigonometric functions can be first assumed, with arbitrary coefficients and arguments. Afterwards, these unknown parameters can be deduced by substituting the assumed general expressions into the ODEs and satisfying the specific boundary conditions considered. It leads classically to a linear equation system whose determinant has to be zero (so as to ensure the existence of a non-trivial solution for buckling modes), what allows one to express finally the sought critical load.

As a pioneering result, one can mention first the classical solution from Timoshenko and Gere (2009) for a beam resting on an elastic foundation with simply-supported boundary conditions. In this particular case, the critical forces P_{cr} write:

$$P_{cr} = \frac{\pi^2 EI}{L^2}\left(n_w^2 + \frac{k_s L^4}{n_w^2 \pi^4 EI}\right) \tag{10}$$

where n_w is the half-wave number of the related buckling mode. The first buckling mode, corresponding to the minimum critical force, is then obtained by minimizing the expression in Equa-

tion (10) with respect to n_w, giving rise to the following solution:

$$n_w = \frac{L}{\pi}\sqrt[4]{\frac{k_s}{EI}} \tag{11}$$

Furthermore, other analytical solutions have been also directly derived for pipes with initial imperfections, using similar energy methods. Assuming an initial lateral deflection w_0, only the governing equation (8) has to be replaced by:

$$EI\left(\frac{\partial^4 w}{\partial x^4} - \frac{\partial^4 w_0}{\partial x^4}\right) + P\frac{\partial^2 w}{\partial x^2} + Q_L = 0 \tag{12}$$

where Q_L stands here for the lateral force which may be related through the soil properties to the lateral displacement of the pipe, possibly in a non-linear way. In such a model, the influence of the imperfections on the governing equation (7) in axial direction is not accounted for.

Karampour et al. (2013a) and Karampour (2018) adopted such an initial imperfection, with a sinusoidal shape ($w_0 = w_{0m}\sin(\pi x/L)$) consistent with simply-supported boundary conditions. Assuming the same buckling mode shape $w = w_m \sin(\pi x/L)$ with a unit half-wave number, they easily obtained the corresponding critical force by substituting this expression into Equation (12). Equations (13) and (14) represent therefore the axial compression force P within the buckled region and the same force P_0 away from it accounting for the bowing effect:

$$P = \frac{L^2 Q_L}{\pi^2 w_m} + \frac{\pi^2 EI}{L^2}\left(1 - \frac{w_{0m}}{w_m}\right) \tag{13}$$

$$P_0 = P + \frac{EA\pi^2 w_m^2}{L^2}\left[1 - \left(\frac{w_{0m}}{w_m}\right)^2\right] \tag{14}$$

3.3.2. Indirect solutions

Instead of directly solving the previous complex high-order ODEs, many other indirect ways have been also widely used to analyze the stability and post-critical response of pipelines under axial compression. On the experimental observations concerning both rail tracks and pipelines, Kerr (1978) and Hobbs (1984) prescribed a series of real buckling shapes, as already discussed in Section 1. For each identified buckling mode, a corresponding equilibrium relation can be deduced in the form of an ODE with a lower order than before. For instance, the following relation holds in the case of Mode 1:

$$\frac{\partial w^2}{\partial x^2} + n^2 w + \frac{m}{8}(4x^2 - L^2) = 0 \tag{15}$$

where $m = \mu_L q/EI$, $n^2 = P/EI$.

Equation (15) can then be solved, together with the practical boundary conditions observed during the lateral buckling of pipelines, both at buckle ends ($M(\pm L/2) = 0$) and buckle center

($\theta(0) = 0$ for symmetry reason). The expression of the pipe deflection is thus obtained:

$$w = \frac{m}{n^4}\left(1 + \frac{n^2L^2}{8} - \frac{n^2x^2}{2} - \frac{\cos(nx)}{\cos\left(\frac{nL}{2}\right)}\right) \qquad -L/2 \leq x \leq L/2 \tag{16}$$

Likewise, the deflection expression corresponding to Mode 2 takes the following form (Taylor and Gan, 1986):

$$w = \frac{\mu_L q L^4}{16\pi^4 EI}\left[1 - \cos\left(\frac{2\pi x}{L}\right) + \pi \sin\left(\frac{2\pi x}{L}\right) + \frac{2\pi^2 x}{L}\left(1 - \frac{x}{L}\right)\right] \qquad 0 \leq x \leq L \tag{17}$$

Meanwhile, still considering Mode 1, the slope at the buckle ends should be zero. By introducing such a boundary condition in Equation (16), the relation $\tan(nL/2) = nL/2$ is obtained, whose lowest non-trivial root turns out to be $nL = 8.9868$.

In the general case, whatever the buckling mode considered, the expression of the axial force P within the buckle (at stable configuration) can be simply expressed as follows:

$$P = k_1 \frac{EI}{L^2} \tag{18}$$

Owing to the flexural shortening effect, the axial force P_0 away from the buckle is increased to:

$$\begin{aligned} P_0 &= P + \tfrac{EA\Delta L}{L} = P + \tfrac{EA}{L}\int_{-L/2}^{L/2} \tfrac{1}{2}\left(\tfrac{\partial w}{\partial x}\right)^2 dx \\ &= P + k_3 \mu_L q L\left(\sqrt{1 + k_2 \tfrac{EA\mu_L q L^5}{E^2 I^2}} - 1\right) \end{aligned} \tag{19}$$

A general expression can also be derived for the maximum amplitude of the buckle w_m and the maximum bending moment M_m, respectively:

$$w_m = k_4 \frac{\mu_L q}{EI} L^4 \tag{20}$$

$$M_m = k_5 \mu_L q L^2 \tag{21}$$

In Equations (18) to (21), the coefficients k_i ($i = 1, 5$) depend on the considered buckling modes. They are not explicitly listed here for conciseness purposes.

Based on the previous analysis, one can further obtain similar results for pipes with initial imperfections. Assuming a geometric imperfection consistent with the retained buckling mode, say Mode 1 for instance, and still using the potential energy method, the axial force P may finally write:

$$P = 80.76 \frac{EI}{L^2}\left[1 - \frac{R_1}{75.6}\left(\frac{L_0}{L}\right)^2\right] \tag{22}$$

where L_0 is the wavelength of the initial imperfection and R_1 is a function of the wavelength ratio L_0/L (Taylor and Gan, 1986).

One of the crucial design parameters for submarine pipelines is the maximum temperature rise

(or the minimum safe temperature rise) ΔT. It can be expressed through the following relation:

$$P_0 = EA\alpha\Delta T \tag{23}$$

The choice of α depends on the steel grade considered. For instance, a value of $1.73 \times 10^{-5}/^oC$ is retained in de Oliveira Cardoso et al. (2015), whereas a value of $1.17 \times 10^{-5}/^oC$ is used by Zeng et al. (2014) and Zhang et al. (2018b). The estimation of ΔT implies therefore the need to calculate the ultimate value of the axial force P_0. There are two possible ways based on the former equations: one solution is to directly minimize Equation (19) with respect to the buckling length L. However, for substantially non-linear problems (when the pipe-soil interaction force is not constant or linear), it is quite impossible to perform this optimization. Consequently, a second solution amounts to use a numerical iterative procedure. A specific numerical case study will be presented in Section 12, for illustration purposes.

4. Effective axial force in a pipeline

4.1. General background

The actual loading conditions exerted on submarine pipelines are complex and vary widely during their entire life cycle. Typical loads include internal pressure, external pressure, bending moments, frictional forces, axial forces, shear forces, and even torsional forces under certain conditions (Bai et al., 1993; Guo et al., 2013; Bai and Bai, 2014a,b). All these solicitations may become predominant, depending on operating conditions. For instance, external pressure turns out to prevail during a dry installation in deep water (Cai et al., 2017). During an hydro-test phase, pipelines suffer from an high internal pressure up to 1.25 times the design pressure, which becomes thus predominant (DNV, 2017c). For a pipe resting on the seabed, axial compression is prevalent due to HT/HP. Among other things, the temperature distribution along a pipeline usually takes hours or days to reach a steady state after the products start to run through it (Alves et al., 2012; Konuk, 2018). The structural responses such as lateral buckling, upheaval buckling and pipe walking are induced accordingly (DNV, 2017a). In practice, the central issue is how to effectively take into account the numerous loads which may affect the buckling of pipelines, in a unified and consistent way.

As a remedy, the concept of effective axial force has been proposed to convert the HT/HP experienced by a pipeline into a compression force. It is a controversial but widely used concept in the domain of pipelines. In the sequel, the concept and definition of the effective axial force that produces lateral buckling of submarine pipelines are recalled.

4.2. Concept and definition

It is quite clear that thermal expansion produces an axial compression force in constrained pipelines. However, it is not that obvious the occurrence of internal pressure also leads to axial compression. Some researchers and engineers have been confused with this idea in the beginning, since it is somewhat counter-intuitive. Palmer et al. (1974) deployed an experimental test on a tube under internal pressure, and demonstrated that a compression does exist under appropriate constraints, producing then a lateral buckling phenomenon.

In DNV (2017c), the effective axial force (denoted by P, with a positive sign in tension), which determines the global response of a pipeline, is defined as a function of the true wall force N, the internal pressure p_i and the outer pressure p_e:

$$P = N - p_i A_i + p_e A_e \tag{24}$$

Figure 5 illustrates the example of a pipe under both external and internal pressures. The loading configuration can be equivalently divided into two components if a virtual end cap is added at the pipe ends (central image). With the new virtual caps, an equivalent axial force ($P_e A_e - P_i A_i$) due to pressures, as seen from the blue and red arrows in the central image, should be introduced for balance reason so that the physical system would not be changed and extra forces would not be added. Hence, *Part* 1 denotes the buoyancy of a submerged pressure vessel and the weight of the displaced water, which are obviously in equilibrium. As a result, this part has no effect on further buckling. Conversely, *Part* 2 denotes the structure under the corresponding effective axial force, which actually produces pipe buckling. The true wall force N is obtained by integrating the axial stress over the cross-sectional area of the pipe. From this value, the effective axial force is actually deduced by accounting for internal and external pressure, so that it can be finally used for the global buckling analysis of the pipeline. In this way, the complex integration on a possibly doubly-curved pipe geometry is circumvented during global analysis.

This concept was adopted by many researchers such as Fyrileiv and Collberg (2005), Fyrileiv et al. (2013) and Vedeld et al. (2014), as well as engineering standards (DNV, 2017a, 2018). As seen in Equation (24), for an unstressed pipe ($N = 0$) with an internal pressure resting on the seabed, it seems obvious that a negative axial force is produced on the pipe due to internal pressure, equivalent to a compression force directly exerted on the pipe ends, and thus likely to induce lateral buckling.

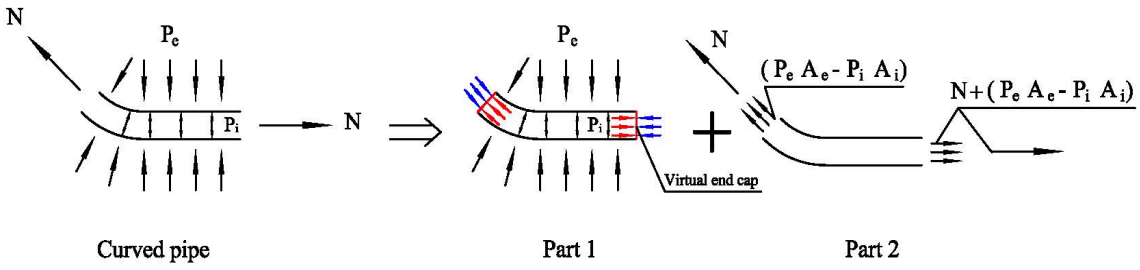

Figure 5: Effective axial force in a pipe subjected to external and internal pressures

5. Influence of initial imperfections

Initial imperfections (such as out-of-straightness) can largely lower the critical buckling loads of submarine pipelines and, as a result, lower the safe temperature differences. Both buckling and post-buckling features will be affected by the occurrence of imperfections. Wang et al. (2017) stated that an increase of initial imperfection induced a decrease of the critical buckling force, but had little effect on the post-buckling response and thus on the final deflection of buckles. However, it has been shown that even a small imperfection could introduce a "snap" phenomenon in the pipeline (Hobbs, 1984; Taylor and Gan, 1986; Liu and Wang, 2018; Wang et al., 2018c,d). In this section, a brief review on the effect of imperfections in the buckling of pipelines is first conducted. Initial imperfections of unstressed and stressed types are successively discussed. The influential parameters related to imperfections are finally presented.

5.1. Research progress related to imperfections in pipelines

Initial imperfections are the toughest characteristics which must be accurately considered in a structural analysis of submarine pipelines. They are mainly due to uncertainties such as misalignment of welded joints, imperfect workmanship or installation procedure, among other things (Konuk, 2018). As far as geometric imperfections are concerned, it is almost impossible in practice to actually measure the real shape of an imperfection, especially for a very long pipeline due to the corresponding workload. Instead, it is commonly assumed that the initial imperfection has the same general shape as one or more buckling modes. In Feng et al. (2015), an initial imperfection in the form of a small arch has been experimentally observed, what confirms the previous hypothesis. Conversely, Zhang et al. (2019) experimentally introduced an initial imperfection in the form of a sinusoidal shape with a single half-wavelength via a pipeline bender. Besides, among others, one can mention Karampour et al. (2013a) who performed calculations using such an initial imperfection with a sinusoidal modal shape.

Basically, there are two types of initial imperfections in pipelines: unstressed imperfections and stressed imperfections (Wang et al., 2018c,d). The unstressed pipe imperfections correspond to local imperfections introduced as a result of factors such as manufacture workmanship without residual stresses. As an example, an unstressed initial imperfection was included in the research of McCarron (2018). Conversely, the stressed pipe imperfections represent the ones produced by external factors such as pipe installation, sway motions of installation ships and uneven seabed (Zeng et al., 2014; Bai et al., 2009). Such global imperfections are produced on initially unstressed pipes, in which residual stresses may appear as a by-product during the associated procedure. However, these residual stresses may not be accounted for. In such a way, the two types of imperfections do not need to be distinguished anymore.

A considerable number of researchers have undertaken studies on the lateral buckling of submarine pipelines with initial imperfections. Dating back to 1984, Hobbs (1984) summarized five typical buckling modes that may occur in the process of lateral buckling of initially perfect pipelines, which were then used by other authors as a basis for the definition of their initial imperfections. Taylor and Gan (1986) took into account such initial imperfections in terms of both their maximum amplitude and half-wavelength. Ju and Kyriakides (1988) and Richards (1990) proved that the critical force of pipelines was also sensitive to the shape of the initial imperfection. In

studies such as Palmer et al. (1990), Maltby and Calladine (1995b), Taylor and Tran (1996) and Croll (1997), the attention was given only to the maximum amplitude of the initial imperfection, which may solely influence the lateral buckling of pipelines. Hong et al. (2015a,b) investigated the case of an initial imperfection in the form of Mode 1 with a single arch.

Furthermore, Karampour et al. (2013a) indicated that the initial curvature of the imperfection was important as well. Zhang and Duan (2015) introduced a shape coefficient ρ_{max}/L_0 in the description of the imperfection. Eight different shapes of initial imperfection (consistent with Mode 1) were then tested for comparison purposes. It was found that an increase of the radius of curvature in the convex area of the initial imperfection could largely increase the critical buckling force of the pipeline. Lastly, Liu and Wang (2018) analytically studied the lateral buckling phenomenon, assuming that pipelines were prone to buckle in Modes 3 and 4, with an initial imperfection of symmetric Mode 1 and anti-symmetric Mode 2, respectively.

5.2. Unstressed initial imperfections

Unstressed initial imperfections are typically introduced by pipe manufacturing process or unexpected accidents such as impacts. The possible residual stresses resulting from these conditions are generally coped with and thus intentionally removed from further analyses. Unlike stressed initial imperfections, unstressed initial imperfections (e.g., impact induced dent) are essentially local geometric imperfections, which may affect therefore the local ultimate strength and buckling stability of small-scale submarine pipelines under certain loading conditions (Cai et al., 2017). In most cases, they take the form of an oval, a lobe or a wave-type imperfection (Bartolini et al., 2014).

The effect of unstressed initial imperfections largely depends on the predominant loading exerted on the pipe. For instance, the effect is insignificant for pipes subjected to pure bending, because the disturbances due to this loading type and the resulting asymmetric deformations are already large enough to cause structural failure (Bai and Bai, 2014b). In contrast, for small-scale pipes under uniaxial compression, local imperfections are prone to decrease the buckling strength by as much as 50% (Song et al., 2004). A typical wave-type local imperfection was measured by Vasilikis et al. (2015) and Es et al. (2016) in an experimental analysis of the buckling phenomenon of a spiral-welded pipe. Cai et al. (2018a,b,c,d) adopted the same type of unstressed initial imperfection, so as to investigate the residual ultimate strength of damaged offshore pipelines. The imperfection amplitude was set to 3% of the pipe thickness.

5.3. Stressed initial imperfections

Stressed initial imperfections in pipelines are generally produced by external factors which mostly originate from the pipe installation. During the installation procedure, an initially unstressed pipe may undergo large global imperfections. As a by-product, non negligible residual stresses are difficult to be removed. The occurrence of stressed imperfections affects then the buckling behavior of the pipeline, namely both the location and the type of buckle, together with the critical load. The classical theory (Timoshenko and Gere, 2009) shows that an elastic perfect beam without imperfections resting on an elastic foundation buckles into an extensive and periodic mode (Mode 5 as described in Section 1). In practice, a buckle localization occurs at an arbitrary place along the pipe, but preferentially close to the ends of the pipeline due to boundary effects. In

contrast, for a real pipe with stressed imperfections, the buckle will inevitably occur at the location of the initial imperfection.

In all cases, as observed experimentally by Hobbs (1984), the real lateral buckling modes resemble sine curves, decaying on either side of a central peak amplitude. As a consequence, in modeling approaches, initial imperfections are assumed to be similar to the real buckled shapes observed in experiments. The type of imperfection naturally determines the final buckling type of the pipeline. As mentioned in Taylor and Gan (1986), when considering initially deformed pipelines, Modes 1 and 2 are more susceptible to appear among all the other identified buckling modes of submarine pipelines. Hence, in numerical computations, Mode 1 is retained as the most likely symmetric initial imperfection:

$$w_0 = \frac{w_{0m}}{K_1}\left(1 + \frac{n_0^2 L_0^2}{8} - \frac{n_0^2 x^2}{2} - \frac{\cos(n_0 x)}{\cos(n_0 L_0/2)}\right) \qquad -L_0/2 \le x \le L_0/2 \tag{25}$$

while Mode 2 acts as the most likely skew-symmetric initial imperfection, as seen in Figure 6:

$$w_0 = \frac{w_{0m}}{K_2}\left[1 - \cos\left(\frac{2\pi x}{L_0}\right) + \pi \sin\left(\frac{2\pi x}{L_0}\right) + \frac{2\pi^2 x}{L_0}\left(1 - \frac{x}{L_0}\right)\right] \qquad 0 \le x \le L_0 \tag{26}$$

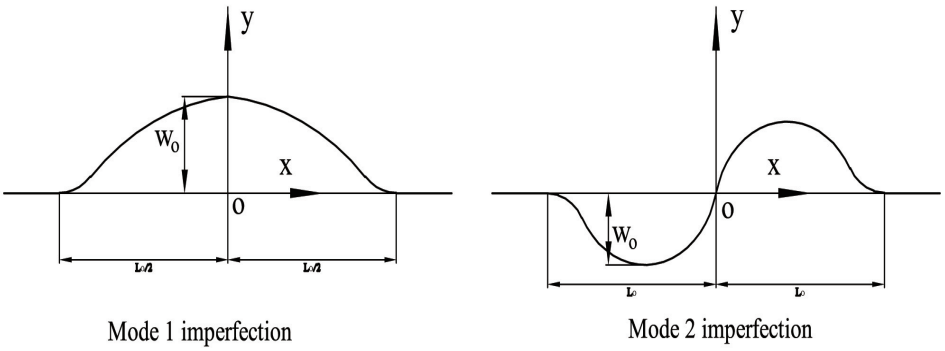

Figure 6: Imperfection shapes in terms of Mode 1 and Mode 2

Therefore, Equations (25) and (26) are classically used for the definition of the initial imperfection in a submarine pipeline, with $K_1 = 15.7$ and $K_2 = 8.62$ according to Equation (20). It should be noted that the amplitude-to-wavelength ratio w_{om}/L_0 remains finally the only feature to fully determine such an imperfection.

Besides, Modes 3 and 4 can be considered as subordinate forms. Similar expressions of initial

imperfections may be derived likewise for these modes:

$$\begin{gathered} w_0 = \frac{w_{0m}}{1.484}\left[1 + 0.484\cos(n_0 x) - 2.109\left(\frac{x}{L_0}\right)^2\right] \\ -L_0/2 \le x \le L_0/2 \\ w_0 = \frac{w_{0m}}{0.821}\left[1 + 0.134\cos\left(\frac{5.836x}{L_0}\right) + 0.031\sin\left(\frac{5.836x}{L_0}\right) - 2.341\left(\frac{x}{L_0}\right) + 1.167\left(\frac{x}{L_0}\right)^2\right] \\ L_0/2 \le x \le 1.295L_0 \end{gathered} \tag{27}$$

$$\begin{gathered} w_0 = \frac{w_{0m}}{8.2}\left[1 - \cos\left(\frac{8.54x}{L_0}\right) + 3\sin\left(\frac{8.54x}{L_0}\right) + 25.74\left(\frac{x}{L_0}\right) - 36.11\left(\frac{x}{L_0}\right)^2\right] \\ 0 \le x \le L_0/1.61 \\ w_0 = \frac{w_{0m}}{0.304}\left[1 + 0.00391\cos\left(\frac{8.54x}{L_0}\right) + 0.05078\sin\left(\frac{8.54x}{L_0}\right) - 2.375\left(\frac{x}{L_0}\right) + 1.3398\left(\frac{x}{L_0}\right)^2\right] \\ L_0/1.61 \le x \le L_0 \end{gathered} \tag{28}$$

where the length L_0 for Mode 4 imperfection in Equation (28) is the half-length of the entire imperfection.

These equations can also be directly used for global buckling investigation.

5.4. Imperfection features

One of the most important features when describing an imperfection is the amplitude-to-wavelength ratio w_{0m}/L_0, as discussed above. Actually, it is the only feature to be defined when one adopts the Hobbs' modes as initial imperfections. In practice, this ratio lies within a particular range when considering initial imperfections in submarine pipelines. Based on McCarron (2018), for an individual pipe with a standard length (12 m) in manufactured mills, the value of w_{0m}/L_0 is normally less than 1/500. Hence, this author proposed a reasonable range of w_{0m}/L_0 between 1/1000 and 1/500 for submarine pipelines. The selection of an imperfection within this range may be appropriate to establish a practical buckling capacity in design.

Other significant features of imperfections in submarine pipelines can be mentioned, such as the minimum curvature of the imperfection shape $1/\rho_{max}$, where the maximum curvature radius of the imperfection ρ_{max} can be obtained from the following geometric expression:

$$\rho(x) = \frac{(1 + w_0{\prime}^2)^{3/2}}{w_0{\prime\prime}} \tag{29}$$

The significance of this parameter was first shown in the context of upheaval pipeline buckling (Ju and Kyriakides, 1988; Maltby and Calladine, 1995a,b; Karampour et al., 2013a). Then, it was also proved relevant in the case of lateral buckling of submarine pipelines. Zeng et al. (2014) found that the critical forces of pipelines could vary depending on this curvature parameter when the amplitude-to-wavelength ratio is incidentally constant. Furthermore, the influence of ρ_{max}/L_0 was analyzed by Karampour et al. (2013a), Zhang and Duan (2015) and Zhang et al. (2018b). Eight different imperfections with various maximum curvature radii were adopted for comparison purposes, as illustrated in Figure 7. For the sake of brevity, only two of these imperfection

expressions are listed here as an example:

$$w_{01} = \begin{cases} w_{0m}\left[\frac{8}{3}\left(\frac{2x}{L_0}\right)^2 - 3\frac{2x}{L_0} + 1\right]\left(1 + \frac{2x}{L_0}\right)^3 & -\frac{L_0}{2} \le x \le 0 \\ w_{0m}\left[\frac{8}{3}\left(\frac{2x}{L_0}\right)^2 + 3\frac{2x}{L_0} + 1\right]\left(1 - \frac{2x}{L_0}\right)^3 & 0 \le x \le \frac{L_0}{2} \end{cases} \tag{30}$$

$$w_{02} = \frac{w_{0m}}{2}\left[1 + \cos\left(\frac{2\pi x}{L_0}\right)\right] \qquad -\frac{L_0}{2} \le x \le \frac{L_0}{2} \tag{31}$$

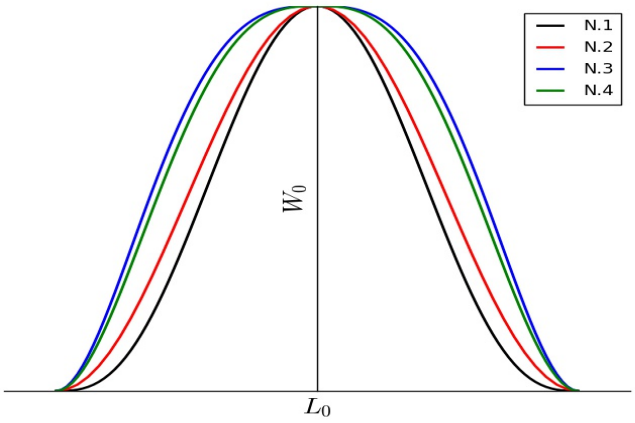

Figure 7: Imperfection shapes in terms of Mode 1 with different ρ_{max}/L_0 (only four curves are shown for clarity reasons) (Zhang et al., 2018b)

6. Pipe-seabed interactions

The pipe-seabed interaction is another crucial factor that will affect the lateral buckling of submarine pipelines. As the foundation of submarine pipelines, the seabed provides them with extra resistance during buckling. This resistance consists of two basic components: friction forces and passive resistance. A common method to account for these effects concerning lateral buckling of pipelines amounts to restricting oneself only to the influence of friction forces, using the well-known Coulomb model (Agusta et al., 2016). However, such a simplification naturally fails to include the passive resistance (Sotberg and Verley, 1992; DNV, 2017b).

In order to facilitate the lateral buckling investigation of submarine pipelines, a comprehensive understanding of the seabed mechanical behavior is necessary. In this section, typical pipe-seabed interaction models found in literature are defined and compared with each other. The most influential parameters related to the seabed properties, such as the initial embedment and friction coefficients, are also discussed.

6.1. Research progress related to pipe-seabed interactions

Figure 8 displays a pipe resting on the seabed and the soil berm it forms when moving due to lateral sweeping, where D is the cross-section diameter, D' is the effective contact width between

the pipe and the soil, u is the lateral pipe displacement, u_{init} is the embedment depth, s_u stands for the undrained shear strength of the soil and A_{berm} is the cross-section area of the soil berm. Owing to the numerous pipe-laying methods and even the possible motions of vessels during laying, the embedment depth of a pipe may significantly vary. As a result, two basic configurations of pipeline penetration are categorized, namely the normal penetration and the over penetration. Once a pipe starts to buckle due to cyclic thermal heating and cooling, a complex pipe-seabed interaction emerges. The pipe is swept back and forth across the seabed accordingly.

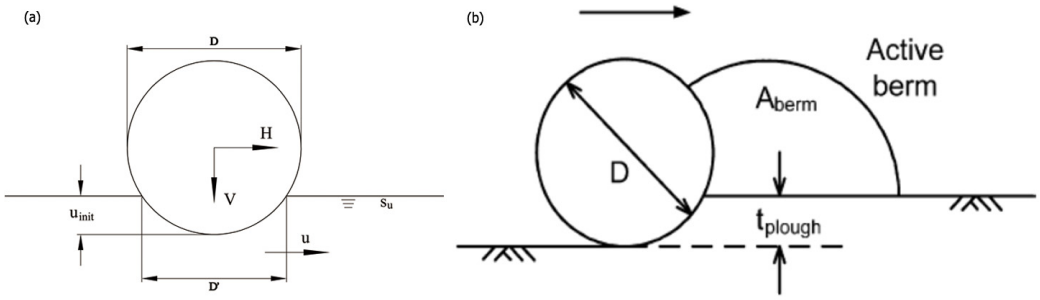

Figure 8: Embedment of a pipe resting on the seabed (a) and the soil berm due to lateral sweeping (b) (White and Cheuk, 2008)

In the original research of Palmer et al. (1974) and Hobbs (1984), a frictional rigid foundation was employed so as to represent the seabed. Soil resistance was thus characterized by the Coulomb friction model with a fully mobilized assumption everywhere. The Coulomb friction force can be expressed as:

$$F_f = \mu q \tag{32}$$

In the same vein, Karampour et al. (2013a) investigated the post-buckling shape of submarine pipelines, with a flat frictional base. This frictional simplification of the seabed was also adopted by other researchers, including Lyons et al. (1973), Karal et al. (1977), Kerr (1978), Anand et al. (1980), Brennodden et al. (1986), Najjar et al. (2007), Safebuck (2008), McCarron (2015a), Wang et al. (2018a) and Liu and Wang (2018).

In reality, the lateral resistance exerted on a pipeline is related to many factors such as the soil strength profile, the pipe embedment and the soil berm effect, among others (McCarron, 2015b, 2017). Wagner et al. (1989), Verley and Sotberg (1994) and DNV (2017b) assumed that this lateral resistance consisted of both a frictional component and a passive resistance. However, the proposed models are only suitable for the modeling of soil resistance in small amplitude. The effect of additional soil berms due to large cyclic motions is ignored. With respect to this aspect, Bruton et al. (2006) identified three specific stages for the description of the pipe-soil interaction based on experiments, including the breakout stage, followed by an unstable movement and a residual stage. Cheuk et al. (2007), Dingle et al. (2008) and White and Cheuk (2008) studied the large amplitude cyclic pipe-soil response based on experimental tests. Wang et al. (2018a) experimentally investigated the lateral soil resistance on shallow-embedded pipelines, using sand from Bohai gulf in the eastern China sea. Some significant features were identified, such as the

breakout resistance $H_{breakout}$, the residual resistance H_{res} and the maximum resistance H_{max}. It was found that, in the case of a deep embedment, $H_{breakout}$ was coupled with both H_{res} and H_{max}.

6.2. Lateral resistance models

6.2.1. Bi-linear models

A bi-linear lateral resistance model is first presented here, which accounts for both the friction component and the passive resistance in terms of soil breakout (Murff et al., 1989; Galgoul et al., 2004). In such models, it is assumed that the lateral soil resistance and the pipe displacement are related through a bi-linear "elastic-perfectly plastic" constitutive law. Figure 9(a) illustrates such a bi-linear response, where the horizontal axis denotes the normalized lateral displacement of the pipe while the vertical axis represents the normalized lateral resistance. Meanwhile, full mobilization is not reached until a given (small) displacement ($u_{breakout}$) due to passive resistance. As estimated by Lyons et al. (1973), Brennodden et al. (1986), Wagner et al. (1989) and BS8010 (1993), the displacement to mobilization is approximately $0.1D$. The soil stiffness k_s before full mobilization can be therefore calculated by $H_{max}/u_{breakout}$. After full mobilization, the lateral resistance phenomenon can be assigned to Coulomb friction. The selection of the frictional coefficient depends on the type of seabed. Pipe-soil experimental tests from Lyons et al. (1973), Lambrakos (1985) and Wagner et al. (1989) showed that the friction coefficients lie in a range between 0.2 and 0.8. A typical value adopted for clay seabed is 0.2 (Sotberg and Verley, 1992; DNV, 2017b). In the numerical simulations of Zhang et al. (2019), a lateral friction coefficient of 0.3 is considered. The Coulomb model is adopted as well when friction is also involved in the axial direction. In Kerr (1978), Najjar et al. (2007), Safebuck (2008) and Zhang and Duan (2015), a value of 0.6 is adopted for the axial friction coefficient, accounting for coating effect.

This model is simple but sufficiently reasonable for use in engineering practice. As stated by McCarron (2018): "The change of buckle capacity is small due to large change of lateral resistance, so it is reasonable to use a perfectly plastic response in preliminary design". Despite this, it is sometimes not accurate enough since the real influence of the vertical load is not accounted for. It manifests itself by the penetration of the pipe in the soil during horizontal movement and thus by a variation of the contact area between pipe and soil.

6.2.2. Tri-linear models

In order to better reproduce the pipe-soil interaction features, tri-linear lateral resistance models were proposed. In these models, both a breakout and a residual resistance are brought into play. After the pipeline breakout, two different behaviors may exist, as seen in Figure 9(b). A hardening response may occur for an "over-penetrated" pipe, whereas a softening response may appear for a so-called "normally-penetrated" pipe resting on the seabed (White and Cheuk, 2008). Wang et al. (2018a) observed that a softening response was likely to happen when the initial embedment was close to $0.5D$, during a large movement of the pipe (larger than $4D$). With a greater initial embedment depth, a hardening response is expected.

Based on experimental tests, Bruton et al. (2006) proposed a specific tri-linear formulation to express the soil resistance on a soft clay seabed for a normal penetration of the pipe, which can be

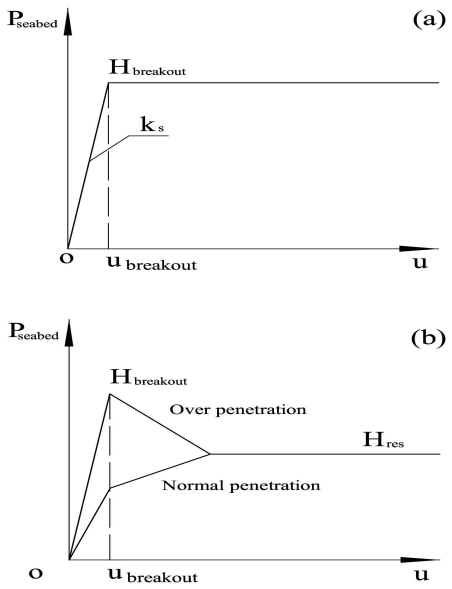

Figure 9: Pipe-seabed interaction models: (a) Bi-linear model; (b) Tri-linear model

summarized by the following equations:

$$\frac{H_{breakout}}{V} = 0.2 + \frac{3}{\sqrt{s_u/\gamma' D}} \frac{u_{init}}{D} \frac{1}{v} \tag{33}$$

$$\frac{H_{res}}{V} = 1 - 0.65\left(1 - e^{-\frac{1}{2}\frac{s_u}{\gamma' D}}\right) \tag{34}$$

In the equations above, $H_{breakout}$ denotes the horizontal force at breakout stage, v is the normalized vertical load ($v = V/Ds_u$), s_u is the undrained shear strength of soil, γ' is the effective soil unit weight and u_{init} is the initial pipe embedment depth. The mobilization distance $u_{breakout}$ corresponding to $H_{breakout}$ is normally in the range of about $0.05D$ to $0.2D$, whereas the mobilization distance u_{res} at the occurrence of the horizontal residual force H_{res} is about $2D$ (Chatterjee et al., 2012; McCarron, 2015a). In DNV (2017b), a value of $0.05D$ is selected for $u_{breakout}$. Wang et al. (2018a) experimentally showed that H_{res} was only depending on the weight of the berm and that the breakout force was occurring when the mobilized distance had reached $0.1D$.

In such a tri-linear model, there are still abrupt changes in soil stiffness, occurring at both the breakout and the residual point. Accordingly, a plasticity-based macro-element model was proposed in Schotman et al. (1987) and Zhang et al. (2002). Agusta et al. (2016) further divided the breakout stage into both an elastic and a plastic regime in order to remedy such limitations. In these conditions, the use of work-hardening plasticity gives rise to a smooth response in terms of stiffness at the transitions between the different stages involved in the interaction phenomenon.

6.2.3. Other simplified models

In Maltby and Calladine (1995a,b), it was found that the localization phenomenon related to pipe buckling in the presence of an imperfection depends more upon the extreme value of soil resistance H_{soil} than upon the exact constitutive law governing the evolution of H_{soil} with respect to the lateral displacement. Hence, an exponential law was simply used by these authors for the description of the lateral soil resistance, as follows:

$$H_{soil} = H_{soil0}\left(1 - e^{\frac{w_0 - w}{\Delta}}\right) \tag{35}$$

where H_{soil0} stands for the limit value of the lateral resistance, and Δ is a constitutive parameter. The authors also suggested some particular values based on experimental tests, namely $H_{soil0} = 3.2\ N/m$ and $\Delta = 1.7\ mm$. In Karampour et al. (2013a), this resistance model was adopted for the analytical investigation of lateral buckling accounting for initial imperfections.

Likewise, the axial soil resistance exerted on a pipeline can also be expressed as a function of fully mobilized coefficients. As an example, the following relation has been employed so as to express the sub-fully mobilized axial friction coefficient in the North sea environment (Bjerrum, 1973; Taylor et al., 1985; Taylor and Gan, 1986):

$$\varphi_A = \mu_A\left(1 - e^{\frac{-25u_s}{u_\varphi}}\right) \tag{36}$$

where μ_A is the fully mobilized axial friction coefficient and u_φ is the corresponding movement at full mobilization. The variation of axial friction forces depends thus essentially on the axial deformations of the pipeline through the value of the resultant longitudinal movement u_s at buckle/slip length interface. The value of φ_A lies naturally in the range from 0 to μ_A. Suggested full scale values for both μ_A and u_φ are 0.5 and 5 mm, respectively (Lyons et al., 1973; Anand et al., 1980; Taylor et al., 1985).

During the lateral buckling of a submarine pipeline, a soil berm (as seen in Figure 8(b)) is prone to appear. As stated by White and Cheuk (2008), the influence of such a soil berm should be considered for pipes with a large horizontal movement (typically between $5D$ and $10D$). The soil berm phenomenon comes from the fact that the pipeline pushes the soil ahead during its lateral movement. Generally, for a light pipe on a stiff seabed which ploughs only a thin layer of material away, the berm will grow slowly. Conversely, for a heavy pipe on a soft seabed which ploughs more soil away, the berm will grow much faster. The occurrence of such berms makes the prediction of the pipe-seabed interaction more complicated (Bruton et al., 2005; Konuk and Yu, 2007). In White and Cheuk (2008) and ISO (2016), simple power laws are used to describe the berm properties, including both the plough depth (t_{plough}) and the normalized horizontal berm resistance (h_{berm}):

$$\frac{t_{plough}}{D} = \alpha\left(\frac{V}{Ds_u}\right)^{\beta} \tag{37}$$

$$h_{berm} = \lambda\left(\frac{A_{berm}}{D^2}\right)^{\delta} \tag{38}$$

where A_{berm}/D^2 represents the dimensionless hardening parameter. α, β, δ and λ are empirical coefficients which can be deduced from experimental tests. For instance, λ is related to the berm size. It is shown that the value of β lies in practice between 2 and 3 (Murff et al., 1989; Verley and Sotberg, 1994). For a rough embedment of the pipe with $u_{init}/D < 0.5$, α and β can be selected as 0.015 and 2.3, respectively (Murff et al., 1989).

When combining the pipe-seabed models described above with the soil berm effects, a more accurate prediction of the pipe-soil interaction can be achieved. For example, an original solution was developed by Zeng and Duan (2014), based on a tri-linear pipe-soil model accounting for extra soil berm effects. It can be described by the following expression of the soil horizontal resistance:

$$H_{soil} = a\frac{\pi}{u_r}u - b\left(\frac{\pi}{u_r}\right)^3 u^3 + \frac{a}{120}\left(\frac{\pi}{u_r}\right)^5 u^5 \tag{39}$$

where u_r is a function of the pipe outer diameter, depending on the soil stiffness, and u is the lateral displacement of the pipe. This modified approach takes into account both the initial penetration (u_{init}) and the berm effects. Parameters a and b are functions of $H_{breakout}$ and H_{res} derived from the tri-linear model. The soil berm effects have been merged into these parameters, through the use of Equations (37) and (38). The use of such a model naturally updates favorably the lateral buckling solution.

7. Residual stresses

Residual stresses can be defined as auto-balancing stresses which are locked into a material when it is free from external forces (Cai, 2018). In submarine pipelines, extensive residual stresses may exist due to many factors such as fabrication, pipe joining processes, welding, heat treatment, mechanical interferences, forming processes and long term service conditions (Jr et al., 1990; Amirat et al., 2004; Pirling et al., 2011). As stated by Taylor and Gan (1986), the influence of residual stresses on the mechanical response of a submarine pipeline can be interpreted like the one of an equivalent initial lack of straightness. However, since stressed imperfections have been already discussed in Section 5, only residual stresses arising from the manufacturing processes will be considered in this section. So far, there is little research on the influence of residual stresses on the lateral global buckling of submarine pipelines.

Residual stresses are known to have a significant influence on the mechanical behavior of building members and tubular offshore structures, among others (Bjoerhovde, 1973; Chen and Han, 1985). For tubes manufactured by means of rolling or welding methods, the effect is relatively small (Galambos, 1998), whereas the effect is greater for offshore pipelines obtained through mill fabrication processes. Toma and Chen (1979) estimated that residual stresses could reduce the buckling capacity of long tubular columns fabricated in such a way by about 2-4%. This effect was shown to decrease with the increase of the pipeline length (McCarron, 2018). Marshall (2013) investigated the axial capacities of welded box and tubular columns. The results also indicated a diminishing influence of residual stresses on the column capacity with an increasing column slenderness. Meanwhile, it is accepted that the influence of lateral geometric imperfections dominates the influence of residual stresses when it comes to the axial buckling capacity of conventionally

fabricated tubular columns (Bjoerhovde, 1973; Toma and Chen, 1979). This phenomenon has been also observed throughout the analysis of a damaged pipe under pure bending, accounting for both residual stresses and initial imperfections (Cai, 2018).

In practice, the BRSL method (Block Removal Splitting and Layering method) can be used to evaluate the residual hoop strain distribution along the pipe thickness (Jr et al., 1990; Amirat et al., 2004). From such experimental measurements, Lynch (1952) deducted an expression for the estimation of the circumferential (or hoop) residual stress. After slitting the pipe longitudinally and measuring the diameter changes, the residual stress can be written as follows:

$$\sigma_r = E_0 t \left(\frac{1}{D_0} - \frac{1}{D_1} \right) \tag{40}$$

where $E_0 = E/(1-\nu^2)$, t is the wall thickness of the pipe, D_0 is its original diameter and D_1 the final diameter after slitting. This method is based on the following assumptions: (i) the material is supposed to be homogeneous and linear elastic (even during layer removal), and (ii) the stresses are uniform along the pipe length.

8. Controlled lateral buckling

The lateral buckling of submarine pipelines is widely investigated in order to reduce the risks of structural failure during their entire life cycle. Uncontrolled lateral buckling normally introduces unexpected and often severe structural damage, largely jeopardizing the structural integrity of the pipelines. The formation of buckles (namely their number, location, shape, as well as the corresponding critical loading) is the key uncertainty in lateral buckling design (Sinclair et al., 2009). Meanwhile, it is not economically feasible to fully restrain the entire pipeline via traditional methods such as rock dumping or burial. Therefore, the question arises of how to reasonably control the occurrence of lateral buckling in submarine pipelines. Broadly speaking, the buckle triggering method has proven to be the best solution to control the thermal buckling of submarine pipelines (Bruton et al., 2005; de Oliveira Cardoso et al., 2015). In this section, the existing buckle initiation techniques will be thus presented, and the current research about them will be discussed.

8.1. Buckles triggered by laying methods

In engineering practice, the buckle initiation can be introduced through pipe laying methods. For instance, the snaked-lay technique allows one to introduce horizontal imperfections in the pipes with given curvature radii at predetermined locations. In other words, snaked-lay pipelines are laid in a series of gentle curves. It is the most common buckle initiation approach employed to date and its success rate in triggering buckles at the prescribed bends is larger than 90% (Sinclair et al., 2009). However, it is very time-consuming and costly (Chee et al., 2018).

8.2. Buckles triggered by sleepers

Another prevailing method in pipeline industry amounts to the use of vertical sleepers (as illustrated in Figure 10), which act as initial imperfections in installed pipelines (Wang et al., 2018d). Sleepers are usually located at the connections between successive pipe segments, and are

installed prior to pipe laying with an appropriate spacing. Owing to the coating deposited outside the sleeper, the friction between the pipe and the sleeper is highly reduced, compared to the pipe-soil friction. Hence, sleepers have the advantage to reduce the critical buckling force and thus to give rise to more benign buckles with lower strain levels. Operational data from nine pipelines with sleepers have shown that it was a reliable way to trigger the desired buckles (Sinclair et al., 2009). In particular, the symmetric buckling modes (1 and 3) and the asymmetric one (2) described above can be produced through the use of sleepers. Vortex-induced vibrations could also be generated as a by-product, depending on the pipe span between sleepers. It has been already observed in practice and should be avoided (DNV, 2017b).

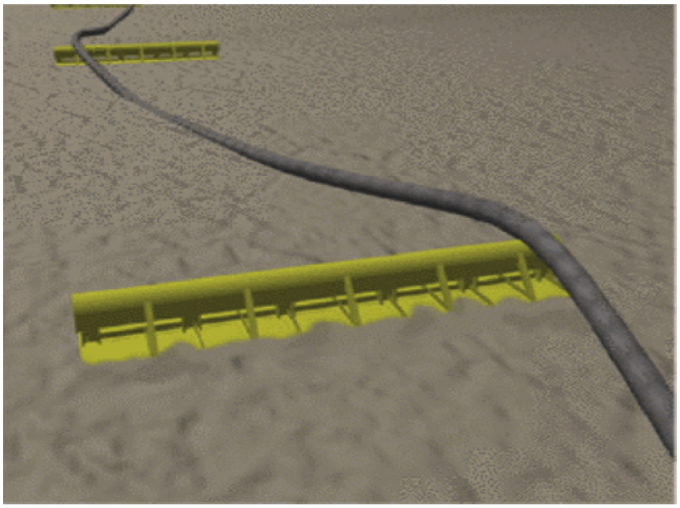

Figure 10: Sleepers used to control lateral buckling of pipelines (Chee et al., 2018)

de Oliveira Cardoso et al. (2015) experimentally analyzed the thermal buckling behavior of submarine pipelines with sleepers and accounting for buoyancy. Two meters long sleepers were adopted with various heights (15 or 30 *mm*) and friction coefficients (0.1 or 0.2). Wang et al. (2017) numerically studied the lateral buckling of pipelines with a sleeper. Empirical formulas in terms of critical buckling force, buckling stress and final displacement were proposed, deriving from the use of genetic algorithms. Wang et al. (2018c) analytically explored the influence of sleepers on the lateral buckling of pipelines. A buckle in the shape of Mode 1 was prescribed. It was found that increasing the height of the sleeper or decreasing the friction between the pipe and the sleeper may reduce the minimum critical loading. Lastly, Wang et al. (2018d) carried on the investigation with a prescribed buckling mode in the shape of Mode 3 (based on energy considerations, it can be shown that Mode 3 is more likely to appear in practice).

As can be seen in Figure 10, the presence of sleepers significantly modifies the mechanical response of pipelines. A variation of friction is intentionally introduced through the use of sleepers. A touchdown point is fashioned between the pipe and the seabed. For a pipeline resting on a sleeper, only a small segment of the pipe is prone to mobilize first under thermal expansion, due to the localized loss of axial friction. Once a lateral buckle is formed at the location of the sleeper, the surrounding part of the pipe feeds into the buckle. Then, the axial compression force drops

within the buckle, pulling more pipe length inside it. This situation is illustrated in Figure 11(b), where the feed-in region extends to a length of $2l_2$ and the slip length is denoted by l_s, P_0 being the axial compression force at virtual anchor points.

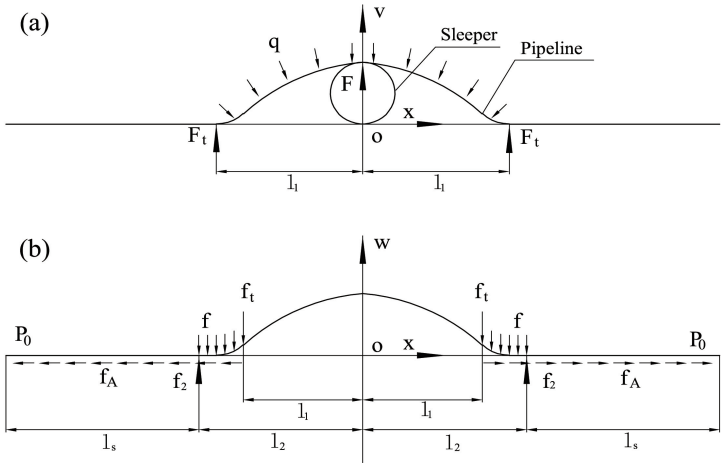

Figure 11: Configuration of a controlled pipeline with a sleeper: (a) vertical plane; (b) lateral plane (Wang et al., 2018c)

In the presence of sleepers, the governing equation (8) may be only slightly updated. A vertical pre-equilibrium equation should be satisfied at the beginning. As shown in Figure 11(a), a uniform distributed force (the pipe self-weight per unit length q) applies on the pipe in the range within touchdown points, even in absence of axial force. Hence, a new governing equation holds in this range:

$$EI\frac{\partial^4 v}{\partial x^4} = -q \qquad 0 \le x \le l_1 \tag{41}$$

A closed-form solution of this equation is not difficult to obtain, when combined with the appropriate boundary conditions at the touchdown point (namely the vertical displacement, the slope and the corresponding moment should be zero). The solution in terms of vertical deflection is as follows:

$$v = -\frac{qx^4}{24EI} + \frac{ql_1x^3}{9EI} - \frac{ql_1^2x^2}{12EI} + \frac{ql_1^4}{72EI} \tag{42}$$

which can be used to determine the touchdown points (that is the span length) as long as the sleeper height is known.

Furthermore, the new expression of the lateral governing equation (8) will be different, varying along the pipe. The pipe zone involved in the buckle development has to be divided into two regions when dealing with the lateral buckling on a sleeper: a region in contact with the sleeper (x between 0 and l_1) and a region in contact with the seabed with friction (x between l_1 and l_2). The governing equations of the pipe lateral stability become then:

$$EI\frac{\partial^4 w_1}{\partial x^4} + P\frac{\partial^2 w_1}{\partial x^2} = 0 \qquad 0 \le x \le l_1 \tag{43}$$

$$EI\frac{\partial^4 w_2}{\partial x^4} + P\frac{\partial^2 w_2}{\partial x^2} + \mu_L q = 0 \qquad l_1 \le x \le l_2 \tag{44}$$

As indicated in Equations (43) and (44), the central part of the buckle is assumed to rest on the sleeper without lateral friction, and there are both a lateral and a vertical concentrated force at the touchdown point (at $x = l_1$). Lateral friction is fully mobilized and uniformly distributed on the remaining part of the pipe. Under these conditions, the general solutions in terms of deflection w_1 and w_2 can be obtained in the following forms:

$$w_1(x) = B_1\cos(nx) + B_2\sin(nx) + B_3 x + B_4 \tag{45}$$

$$w_2(x) = C_1\cos(nx) + C_2\sin(nx) + C_3 x + C_4 - \frac{\mu_L q}{2n^2 EI}x^2 \tag{46}$$

where $n^2 = P/EI$, B_1 to B_4 and C_1 to C_4 being coefficients to be determined using the proper boundary conditions consistent with the presence of a sleeper. In this case of controlled buckling with a sleeper, a compatibility condition is also needed, which relates the extra length of the pipeline in the buckled region ($u = \frac{1}{2}\int_0^{l_1}(\frac{\partial w_1}{\partial x})^2 dx + \frac{1}{2}\int_{l_1}^{l_2}(\frac{\partial w_2}{\partial x})^2 dx$) with the axial expansion (due to the axial force) of the pipe between the virtual anchor points.

8.3. Buckles triggered by buoyancy

The distributed buoyancy technique can also be applied for the initiation of buckles in submarine pipelines. One solution is to introduce vertical imperfections during the laying procedure, while the other solution is to provide locally a lower submerged weight during operation. In any case, a buckle is expected to take shape at the desired location (Shi and Wang, 2014). Generally, the length of the buoyancy section is about 60 m to 200 m with a weight variation of 10 to 15% of the nominal self-weight of the pipe (Sinclair et al., 2009).

Peek and Yun (2007) analytically studied the influence of a single-point, a two-point and a distributed buoyancy load on the lateral buckling of pipelines. A similar analysis was performed by Shi and Wang (2014), but only in the conditions of a single buoyancy load. Wang et al. (2018b) analytically investigated the case of distributed buoyancy sections. The influence of various buoyancy parameters such as the length and weight, as well as the effect of initial imperfections, were discussed. It was found that the minimum critical load (or temperature difference) reduced with the increase of the buoyancy length and the decrease of its weight ratio.

A survey project involving three BP's operational pipelines has been conducted to determine if these buckle initiation techniques are reliable in practice (namely if the buckles form as planned by the methods discussed above) (Hoor et al., 2014). The results demonstrated the effectiveness of such initiation strategies. All the planned buckles for the two inspected pipelines were successfully formed at both sleeper and buoyancy sites, with a Mode 1 shape. Unplanned buckles were observed as well, which indicates that further investigation is still needed to fully control the initiation of buckles. The capabilities of the current methods to predict the locations and behaviors of buckles are still not sufficient (Konuk, 2018).

9. Numerical simulation of pipe lateral buckling

Numerical simulation is a perfect alternative for the investigation of lateral buckling at the time when analytical methods cannot provide accurate estimations under complex conditions. Moreover, numerical computations deliver results which can be further used for empirical predictions. Therefore, in this section, the numerical methods classically used for the lateral buckling analysis of pipelines are presented and discussed.

A considerable number of numerical works have been undertaken so far concerning the global lateral buckling of submarine pipelines. Miles and Calladine (1999) used Abaqus software for the simulation of experimental tests devoted to the lateral buckling of pipelines (Abaqus6.17, 2017). Hoor et al. (2014) elaborated specific numerical models with short virtual anchor spacings for the controlled buckling analysis of submarine pipelines. In their analysis, soil berms were accounted for using non-linear springs. Liu et al. (2014) compared four different numerical methods for the simulation of global buckling of pipelines, namely 2D/3D implicit and explicit methods. Zeng et al. (2014) numerically studied the upheaval buckling of buried pipelines with initial imperfections by using a 2D model. Zhang and Duan (2015) evaluated the critical force of upheaval buckling of pipelines with an initial imperfection of Mode 1 shape. Wang et al. (2017) numerically investigated the lateral buckling of pipelines accounting for both initial imperfections and sleepers (using a so-called pipeline-sleeper-seabed numerical model). Zhang et al. (2018b) analyzed, still numerically, the influence of initial imperfections on the lateral buckling force. They found that the shape parameter ρ_{max}/L_0 had a strong effect on the critical force. In addition, Zhang et al. (2018a) adopted a 2D model to determine the critical force of submarine pipe-in-pipe pipelines on a soft foundation with symmetric initial imperfections.

9.1. General finite element modeling of pipelines

Most of numerical investigations in pipeline buckling analyses make use of the finite element method. Among the available commercial softwares, Abaqus is certainly the most adopted for the numerical simulation of pipeline buckling. Owing to the fact that a pipeline is an ultra-slender structure, it is generally modeled with Timoshenko beam elements. For instance, 2D PIPE21 elements, which are two-node linear elements allowing for transverse shear deformation in a 2D modeling space, were deployed by Zeng et al. (2014). A 3D modeling space is also adopted for the sake of accuracy. For instance, Agusta et al. (2016), Wang et al. (2017) and Zhang et al. (2018b) used standard PIPE31 elements, while Van den Abeele et al. (2015) and Chee et al. (2018) used hybrid PIPE31H elements, both for global buckling analyses. Such hybrid elements have one or two additional nodal variables related to the hoop strain of the pipe wall, and still use linear interpolation. They are well suited for problems involving contact, such as the laying of a pipeline in a trench or on the seabed, or the interaction analysis between a drill string and a well hole, and all the more so in dynamics (in the event of impact, for example). Similarly, using Ansys software, Karampour (2018) deployed both BEAM188 and PIPE288 elements in the context of pipe buckling investigations.

Besides the proper selection of the finite element types, the mesh density is crucial to ensure the accuracy of a numerical simulation. A mesh sensitivity analysis is normally required. In Zeng et al. (2014), it was found that the simulation results tend to converge when a density of

one element per meter is reached. In Zhang et al. (2018b), this strategy was therefore adopted for pipeline buckling analyses, using for instance 1200 elements for pipes with a length of 1200 m.

The selection of the pipeline length to be considered in the model is another important aspect during numerical investigation of pipe buckling. As emphasized by Ju and Kyriakides (1988), the lateral buckling of pipelines is necessarily characterized by a localization phenomenon. That is to say, the buckling response of a pipe only manifests itself in a certain interval length, and does not influence thus the entire structure. Generally, the region of the pipe between the virtual anchor points is only retained for investigation. The total length considered is therefore the sum of the buckle length and the slip length. In practice, the slip length is long enough so that the boundary conditions do not affect the central buckling response.

In numerical computations, the seabed is normally modeled as a rigid foundation for simplicity purposes. For instance, Zhang et al. (2018b) made use of R3D4 rigid elements (from Abaqus software) so as to mimic the seabed as well as the sleepers, as seen in Figure 12(a). In this way, the penetration and embedment of the pipe in the soil foundation cannot be realized. In order to account for these phenomena, if computational resource is sufficient, 3D solid elements can be used in pipe buckling analyses. Among others, Liu et al. (2014) adopted the Mohr-Coulomb model so as to describe the real soil behavior through C3D8R solid elements (from Abaqus software), as shown in Figure 12(b). Some specific soil properties, such as the bulk density λ' (in N/m^3), the compression modulus E' (in Pa), the cohesive coefficient C (in Pa) and the internal friction angle ϕ, were therefore introduced in the model. In Hong et al. (2015b), C3D8R solid elements were also used for the seabed representation.

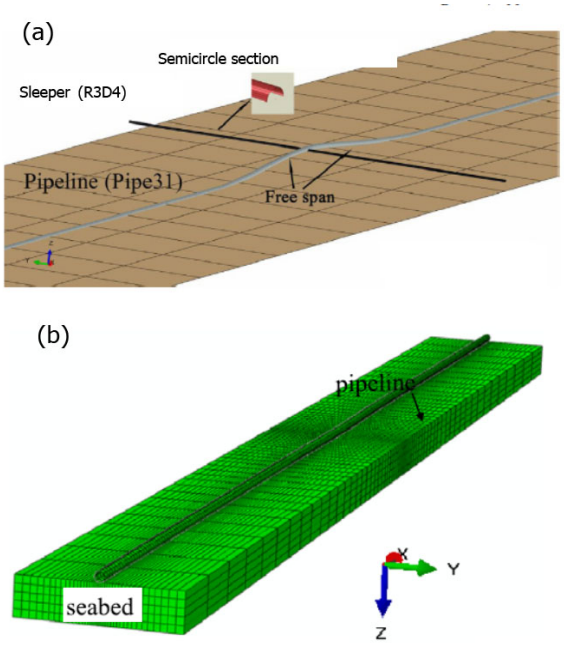

Figure 12: FE models of pipelines for lateral buckling analyses: (a) rigid seabed representation (Zhang et al., 2018b); (b) 3D seabed model (Liu et al., 2014)

9.2. Computational algorithms in numerical simulation

9.2.1. Newton-Raphson method

Most of numerical computations performed in the context of pipeline lateral buckling turn out to be incremental non-linear calculations, since linearized stability analyses are most often not feasible due to some non-linear features in considered models. Therefore, the classical Newton-Raphson iterative method can be used to solve non-linear equilibrium equations (Traub, 1982). Many examples of studies using Newton's method for pipeline simulation are available in literature. Among others, one can mention Zeng et al. (2014), who investigated the upheaval buckling of pipelines with initial imperfections using Newton's method. In a slightly different way, Zhang et al. (2018b) adopted the static damping method for the analysis of pipelines.

Unfortunately, this method is prone to fail once a critical point (namely a bifurcation or especially a limit point) is reached, since the load is generally not increasing any more after such a point and cannot be thus incremented indefinitely. In such a case, which is quite commonly encountered in pipe buckling analyses, alternative approaches can be applied.

9.2.2. Modified Riks method

In order to overcome the drawbacks of Newton-Raphson method, Riks (1972, 1979) developed the arc-length method, which can deal with limit points and non-monotonous equilibrium curves, and thus easily capture the buckling/post-buckling behavior of any structure. The so-called modified Riks method is an algorithm that allows to get an effective solution for such cases (Riks, 1979). In order to circumvent the failure of the calculation due to the non-monotonous evolution of the external load (and/or displacement), an extra arc-length parameter is introduced, related to both the load and the displacement, which can be viewed as the length of a particular load-displacement curve plotted in the appropriate space of finite dimension (defined according to the finite element discretization). The basic algorithm still relies on the Newton's method, but a more efficient path-following technique is used by incrementing the arc-length instead of the enforced load or displacement. This method has proved to be effective for proportional loadings and reasonably smooth structural responses without sudden bifurcations.

The standard numerical procedure for the lateral buckling analysis of pipelines based on the modified Riks method can be summarized as follows:

(a) An eigenvalue buckling analysis is first conducted to calculate linearized buckling modes, further used as initial imperfections (instead, a dead load can be initially applied which may also act as an initial imperfection).

(b) A reference load (including magnitude and direction) is added into the model. The first critical value obtained through the linearized buckling analysis can be used as the reference load.

(c) The current applied load is related to the reference load by the load proportionality factor. The initial arc-length increment is defined. If necessary, the geometric and material non-linearities are taken into account in the simulation.

(d) Finally, the arc-length is incremented and the corresponding load is updated at each increment and proportionally applied on the structure, until the termination conditions (such as a maximum arc-length) are reached.

In summary, the modified Riks method can accurately capture the effects of tiny characteristics such as initial imperfections, whereas the traditional Newton's method cannot do so. Thus, for pipelines under uniaxial compression which are very sensitive to the occurrence of initial imperfections, it is recommended to use the modified Riks method. For pipelines under pure bending, which are less sensitive to such imperfections, both the Newton's method and modified Riks method can be adopted.

9.2.3. Explicit dynamic method

In the case of a sudden snap-through or snap-back phenomenon (involving a sharp limit point), a dynamic method can be employed so as to capture both accurately and efficiently the unstable response of the structure. On one hand, by using an explicit dynamic method, there is no more need to solve large stiffness matrices. On the other hand, an explicit solution procedure is conditionally stable, which means that the time increment cannot exceed the limit stable time $\Delta t_{stable} = 2(\sqrt{1+\xi^2}-\xi)/\omega_{max}$, where ω_{max} is the supreme natural frequency and ξ the corresponding critical damping. Therefore, an explicit numerical scheme requires numerous time increments, but the computation time required for each time increment is very small.

Such a dynamic method has been already implemented in a considerable number of numerical simulations in the literature dealing with pipeline lateral buckling. As an example, Van den Abeele et al. (2015) analyzed the buckling behavior of a 10 *km* long pipeline, by means of Abaqus software. A transient dynamic (explicit) solver was used with a mesh size of 4 *m*. Hong et al. (2015b) adopted an explicit dynamic procedure (via Abaqus) so as to simulate the non-linear response of a pipeline of length 2000 *m*, diameter 323.9 *mm* and thickness 12.7 *mm*. During the simulation, the gravity force was first applied, shaping an interaction between the pipeline and the seabed. Then, in the initial time increment, the temperature in the pipeline was set to zero. The total temperature difference was applied in the second time increment. Besides, Agusta et al. (2016) performed a dynamic analysis for the investigation of pipe walking, using PIPE31 and PIPE33 elements (in Abaqus). Finally, Wang et al. (2017) developed a pipeline-sleeper-seabed model within Abaqus. A dynamic method was adopted as well, with the use of PIPE31 elements and encompassing geometric non-linearities. Simply-supported boundary conditions were enforced at both ends of the pipe of length 2000 *m* and a hard contact model was selected.

10. Experimental analysis of pipe lateral buckling

Numerical simulation is certainly the most efficient way to predict the buckling response of submarine pipelines, when analytical solutions are no more available, particularly in the presence of geometric and material non-linearities. However, it cannot replace experimentation since, in pure numerical simulation, owing to the modeling hypotheses/simplifications, there is a risk of ignoring small but important features, which may be crucial for the description of the actual physical phenomena. Therefore, experimental investigations of the lateral buckling of pipelines have been undertaken in past decades, which will be presented and discussed in this section.

To date, a considerable number of experimental tests have been conducted on the lateral buckling of pipelines. Palmer et al. (1974) realized a simple experiment to demonstrate the influence of internal pressure on the pipe buckling behavior. A straight thin-walled stainless steel tube, with

a length of 1865 *mm* and a diameter of 7.8 *mm* was fixed by steel blocks via cement. It was free to move laterally with the support of thin steel strips. A manual pump was installed for the control of internal oil pressure. The occurrence of a lateral buckle was observed under an internal pressure of 4.9 MPa. In order to study the thermal-induced compression of pipelines, Miles and Calladine (1999) designed a small-scale experimental test (see Figure 13), using a silicone rubber strip (of 2 *m* long) to mimic a pipe. Both the elastic and frictional properties of the silicone rubber strips were taken into account. A lobe extinction phenomenon was then observed. de Oliveira Cardoso et al. (2015) experimentally investigated the controlled thermal buckling of submarine pipelines. Sleepers and distributed buoyancy were used to trigger the lateral buckling phenomenon. An oil export pipeline with a length of 195 *m*, a diameter of 18 *in* and a diameter-to-thickness ratio $D/t = 15.9$ was retained. The ends of the specimen were fixed and a pump was included in the experimental setting so as to produce high pressures and high temperatures. The length of the sleepers was 2 *m* whereas their height lay between 15 and 30 *mm*. The related tests were beneficial for the study of design conditions in terms of trigger spacing and properties, and buoyancy efficiency, among others. The experimental results obtained in this paper were reused by Wang et al. (2018b) in their analytical study of the controlled buckling of submarine pipelines.

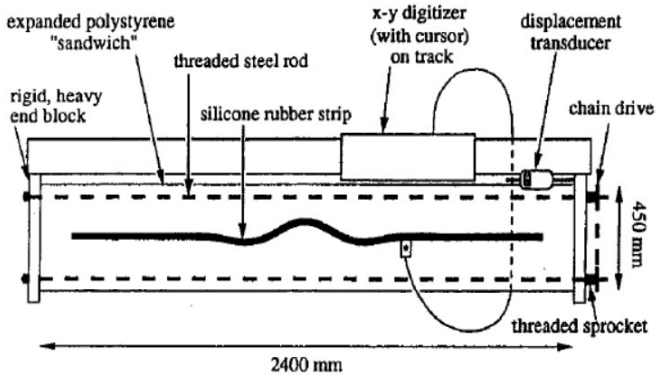

Figure 13: Experimental set-up of a small-scale test of a pipe lateral buckling due to thermal effects (Miles and Calladine, 1999)

Another meaningful example of experimental test has been performed by Zhang et al. (2019), who designed a lateral buckling set-up for a pipe-in-pipe (PIP) structure. Although we do not concentrate on this particular type of pipe in this paper, the experimental method involved can be used under more general conditions and be served as a good reference. As seen in Figure 14, the pipe specimen in hand was made of aluminum alloy, had a length of 9 *m* and rested on a sand tank. The pipe ends were fixed longitudinally via an end fastening device, whereas the rotations were not constrained. An initial imperfection of sinusoidal shape (with a single half-wavelength) was introduced using a pipeline bender. Different half-wavelengths L_0 and amplitudes w_{max} were produced. An oil temperature control loading device was used, allowing for a gradual monotonous temperature increase. Let us finally mention other experimental works on this subject, dealing with the vertical buckling of buried pipelines (Maltby and Calladine, 1995b; Liu et al., 2015), the global lateral buckling (Taylor and Tran, 1996) and the detection methods of the lateral buckling of pipelines (Feng et al., 2015).

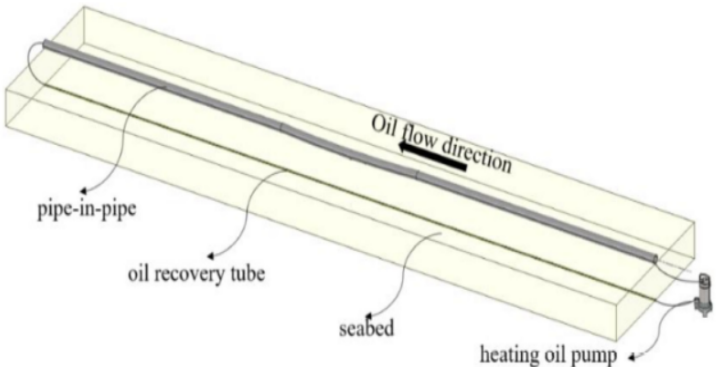

Figure 14: Schematic layout of a pipe lateral buckling test (Zhang et al., 2019)

As shown in Cai et al. (2019) from experimental tests on damaged pipelines under bending moments, the presence of local damage in pipes may easily lead to the final failure of the pipe, due to the phenomenon of buckling propagation. In practice, an initial damage such as a dent or corrosion on the pipe wall (Cai et al., 2017), as well as an initial imperfection, such as the ovalization of the pipe section (DNV, 2017c), triggers the buckling phenomenon, and even a local mode may then quickly propagate and damage a long segment of the pipeline, or even the pipe in its entirety (Karampour et al., 2013b), leading thus to collapse. Karampour and Albermani (2014) conducted an experimental test in order to investigate such an interaction between lateral and/or upheaval buckling and damage propagation in deep sea. It confirms that clarifying the pipe buckling mechanism can be effectively of great help in avoiding such possible failures.

11. Empirical methods in pipe lateral buckling

The classical theories described above have been shown to be capable of providing fundamental solutions for the buckling strength of submarine pipelines, at least if one assumes an elastic constitutive behavior and remains within the framework of small transformations. However, such models generally overestimate the carrying capacity of practical metallic pipes. From an analytical point of view, it is difficult to account for the effect of all practical parameters, due to obvious mathematical barriers. This section summarizes different procedures which may be used to properly define empirical relationships between the buckling of pipelines and the corresponding influential parameters. Some prediction models devoted to lateral buckling and resulting from these analyses are discussed as well.

A typical method used to build empirical relationships between influential parameters and buckling properties relies on the Buckingham theorem (or Π theorem) (Pankhurst, 1964; Sonin, 2001). This theorem is based on a non-dimensional analysis, whose parameters only relate to the fundamental dimensions, typically among the length, mass and time (according to the well-known MLT unit system). A set of $n-m$ non-dimensional parameters ($\Pi_1, \Pi_2, ..., \Pi_{n-m}$) is defined for the physical problem in hand, deriving from the n relevant variables and considering the m fundamental dimensions brought into play. Such a method is classically used in the domain of fluid mechanics, for the derivation of the dimensionless Reynolds number, for example (Cai et al.,

2010). In Miles and Calladine (1999), it was employed in the context of the lateral buckling of pipelines. Expressions of buckling properties were obtained in this way with respect to some dimensionless parameters, with the objective to match with available experimental and simulation results, circumventing thus the direct resolution of stability equations.

Once basic relationships between buckling properties and relevant parameters are known, prediction models can be further fitted. The traditional linear/non-linear regression analysis has been adopted in the context of pipeline buckling. For the purpose of ultimate strength prediction, Cai et al. (2018a,b,c,d) proposed empirical formulas based on non-linear regression analysis, involving different types of structural damage of pipelines. Nevertheless, the application domain is limited due to small data sets. Zeng et al. (2014) established an empirical formula of the following form:

$$P_{cr} = g\left(\frac{w_0}{L_0}\right)(q^2 EI)^{1/3} \tag{47}$$

where the critical buckling load of the pipeline is a function of independent influential parameters such as the load q, the pipe bending stiffness EI and the imperfection shape feature w_0/L_0. The dimensionless function $g\left(\frac{w_0}{L_0}\right)$ was further fitted, based on numerical simulation data. Last, Zhang and Duan (2015) and Zhang et al. (2018b) considered the influence of an initial imperfection on the lateral buckling of pipelines with an extra imperfection parameter ρ_{max}/L_0. Through the Buckingham theorem again, the previous relation was re-constructed as follows:

$$P_{cr} = g\left(\frac{w_0}{L_0}, \frac{\rho_{max}}{L_0}\right)(q^2 EI)^{1/3} \tag{48}$$

Meanwhile, genetic programming (GP) algorithms provide an alternative for the development of prediction models in the framework of pipeline buckling. Such methods have been also successfully applied for the more general prediction of the structural strength of pipelines (Nazari et al., 2015). Among others, Wang et al. (2017) proposed formulas based on GP for the buckling load/stress and the critical displacement of pipelines with initial imperfections and sleepers. Uniform distributions of the key parameters, such as the bending stiffness EI, the pipe diameter D, the pipe unit weight q and the temperature T, were introduced as the inputs of the method. This example clearly proves that these empirical methods allow one to obtain explicit expressions of the pipeline buckling properties and thus constitute an efficient alternative to the direct mathematical procedures.

Large limitations still exist in the utilization of the above-mentioned empirical formulas, due to limited generalization ability. The proposed formulas are not able to be applied when the pipe conditions and environment are changed. Therefore, a more advanced prediction method for the buckling of pipes is needed. The past few years have witnessed the digitalization of different industry fields and the booming of machine learning and artificial intelligence (Xie and Tian, 2018; Bishop, 2006). Applications of machine learning have been successfully demonstrated in different fields such as autonomous driving, language translation and speech recognition (LeCun et al., 2015; Haghighat et al., 2020). Machine learning has also been initially applied in engineering fields, including solid mechanics (Ghaboussi and Sidarta, 1998), fluid mechanics (Fukami et al.,

2020) and structural health monitoring (Sen et al., 2019). Dealing with pipelines, preliminary work has been also started in terms of pipe strength prediction (De Masi et al., 2015; Ossai, 2020; Chin et al., 2020; Gholami et al., 2020; Cai et al., 2020). However, the majority of pipeline research still largely relies on physical-based methods with a possible feature leaking. The investigation of the data-driven methods on buckling and strength prediction of pipelines is not enough. Meanwhile, the stumbling block remains the need for sufficient data that is crucial for accurate predictions by machine learning methods.

12. Case study

This last section focuses on an important feature related to pipeline buckling, namely the consideration of variable axial friction effects between the pipe and the seabed, through a specific case study. As stated in McCarron (2018), the pipe-soil axial interaction forces should be included in the buckling analysis of long pipeline systems. Generally, a full mobilization of the pipe on the seabed is assumed in most studies, so that both the lateral and axial friction forces are chosen to be constant during the buckle growth. However, practical experiments show that the friction forces are deformation-dependent, as can be seen in Equation (36) in Section 6. The problem is investigated here analytically, in order to measure the influence of such variable axial friction on the lateral buckling of pipelines.

Two different cases are compared, namely one considering variable axial friction and the other one with constant axial friction, all other things being equal. In the former case with variable axial frictional forces, one can directly use the following equations, derived by Taylor and Gan (1986), for the numerical calculations:

$$P_0 = P + \left[2\mu_A qAE\left(\frac{1-e^{-25u_s/u_\varphi}}{25/u_\varphi} - u_s\right)\right]^{1/2} \tag{49}$$

$$u_s = \frac{(P_0 - P)L}{2AE} - 7.9883\times10^{-6}\left(\frac{\mu_L q}{EI}\right)^2 (L^7 - L_0^7) \tag{50}$$

which appear to be highly non-linear, requiring thus a numerical iteration method for the resolution. In practice, given a series of buckled lengths L, the buckling force P_0 and the longitudinal displacement u_s are first solved iteratively. Then, the force within the buckle P and the corresponding temperature increase ΔT are calculated through Equations (22) and (23), respectively. In the latter case with constant axial frictional forces, the axial friction coefficient φ_A becomes μ_A and the same equations can be used. The buckling force P_0 is simplified as follows:

$$P_0 = P + (-2EAq\mu_A u_s)^{1/2} \tag{51}$$

Then, by replacing the expression of u_s (Equation (50)) into Equation (51), one can easily express P_0 as a function of the buckling length L and the initial imperfection length L_0, namely:

$$P_0 = P - \frac{\mu_A qL}{2} + \frac{1}{2}\left[\mu_A^2 q^2 L^2 + 6.39064\times10^{-5}\frac{\mu_A\mu_L^2 q^3 A}{EI^2}(L^7 - L_0^7)\right]^{1/2} \tag{52}$$

Table 1 lists the specific pipeline parameters used for the analytical comparison. It is assumed that the pipe has an initial imperfection in the shape of Mode 1, as described by Equation (25), leading thus to a final buckled shape of Mode 1 type. The imperfection ratio (w_{0m}/L_0) is successively prescribed to 0.003, 0.007 and 0.01.

Table 1: Pipe parameters for the case study

Parameters	Value
Pipe outer diameter D (mm)	650
Pipe wall thickness t (mm)	15
Pipe effective weight q (N/mm)	3.8
Thermal expansion coefficient α $(/^oC)$	1.1e-5
Lateral friction coefficient μ_L	1

Figure 15 displays the comparison of forces P and P_0 for pipes with different initial imperfections, plotted with respect to the buckling amplitude w_m. Axial friction is considered in both cases, in the forms of variable and constant axial friction, respectively. With the increase of the buckling amplitude, the force P within buckle decreases due to the release of thermal expansion. However, the buckling force P_0 generally increases with the buckling amplitude. In the case of a small imperfection only (for instance, with $w_{0m}/L_0 = 0.003$ in Figure 15(b)), a snap-through phenomenon may occur and, therefore, the buckling force decreases just after having reached a limit point and increases again shortly after. The snap-through phenomenon gradually disappears with the increase of the imperfection amplitude. Figure 16 displays the comparison of other buckling features, namely the temperature variation and the maximum compressive stress, again for pipes with different initial imperfections. Small oscillations appear in the curves due to problems of numerical instability encountered during the iterative procedure. Similarly to the buckling force, the temperature rise attains a maximum value when considering the lowest initial imperfection ratio. The other cases with larger imperfections do not reveal such a snap-through phenomenon, but instead a stable post-buckling path. Conversely, the maximum compression stress within the buckle always increases with the buckle amplitude, exceeding the elastic range of the material rapidly.

The interesting point here is that, whatever the parameter considered, in both Figures 15 and 16, ignoring the variation of practical axial friction forces does not affect the final accuracy of the results. Instead, as shown in Figures 15(b) and 16(a), numerical instabilities occur when introducing variable axial friction, due to the higher non-linearity of the equations. Therefore, in these circumstances, it is better to deploy a constant axial frictional coefficient instead of a variable one during the analysis of pipeline buckling, for stability purposes.

13. Conclusive remarks

This paper has reviewed the latest research pertaining to the lateral buckling of submarine pipelines under HT/HP. The lateral buckling is basically a global buckling phenomenon for pipelines resting on the seabed, which may trigger severe structural failure modes. Hence, in past decades,

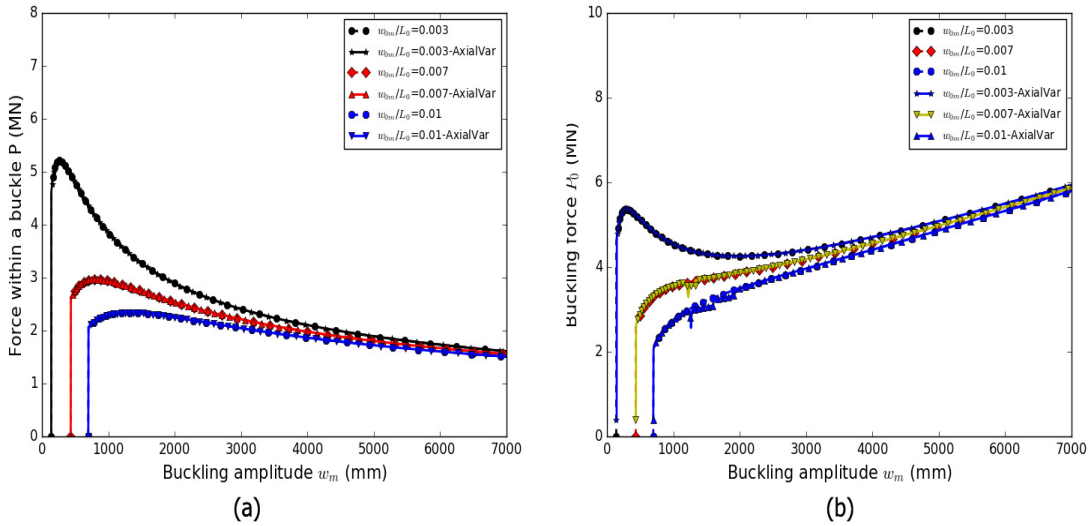

Figure 15: Force variation diagrams with respect to the buckling amplitude w_m of pipes with different initial imperfections: (a) force within buckle P; (b) buckling force P_0

.

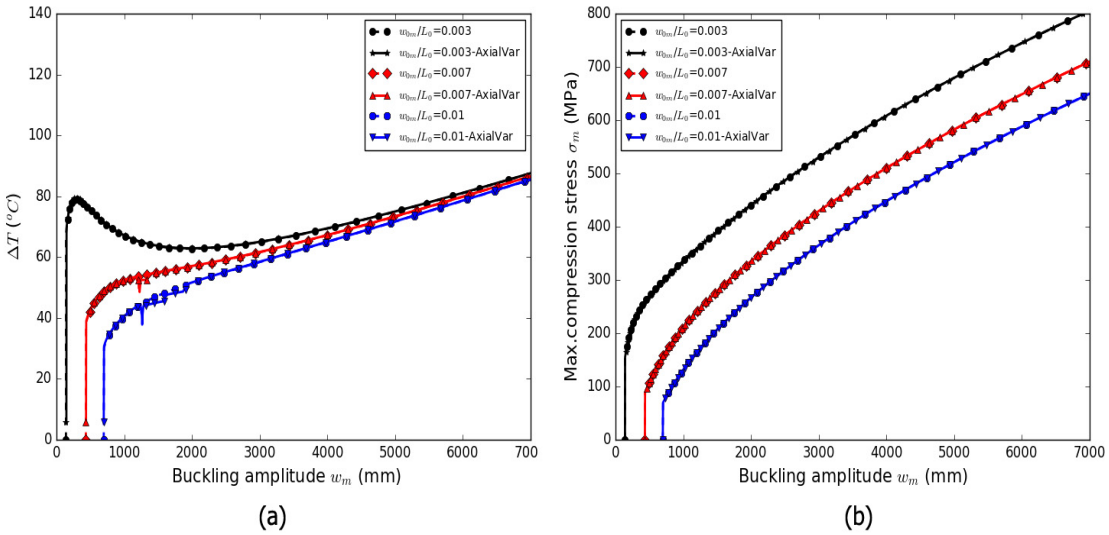

Figure 16: Diagrams of buckling features with respect to the buckling amplitude w_m of pipes with different initial imperfections: (a) temperature variation ΔT; (b) maximum compression stress within buckle σ_m

.

the lateral buckling of submarine pipelines was the subject of considerable interest in many related industries. This paper was an opportunity to record and clarify the main past and current achievements related to lateral buckling, which are available in the literature. In the present paper, the theoretical foundations of the lateral buckling and post-buckling propagation of pipelines have been first introduced. The classical governing equations and the corresponding existing analytical solutions have been particularly recalled. Next, several fundamental aspects related to pipe lateral buckling have been summarized and discussed, including the concept of effective axial force, the influence of initial imperfections and/or residual stresses, the predominant role of pipe-seabed interactions as well as the practical methods of buckle triggering. Experimental methodologies classically used under this context have been also reported. Alternatively to analytical solutions, which may be limited to simplified configurations, suggesting some very strong modeling assumptions, numerical methods have been described together with empirical techniques. Finally, a specific case study has been conducted, based on former analytical expressions derived in the case of pipes with initial imperfections, and devoted to the analysis of the influence of axial friction on the buckling response of the pipes. It has been found that ignoring the axial friction variations does not affect the buckling results (critical force or temperature rise). Instead, it allows one to improve the computing efficiency during buckling analysis.

Based on this review, the remaining areas related to the lateral buckling of pipelines that need to be further investigated have been determined and new challenges concerning submarine pipelines have been identified. The main findings and added values are as follows:

- Torsional effects are generally ignored in lateral buckling analyses, primarily because of the large slenderness of the pipelines in practice. However, torsion may have a non negligible influence on the buckling features, especially when the buckling phenomenon occurs during installation or operation stages due to the uneven seabed. Such torsional effects on the lateral buckling of submarine pipelines have not been quantified so far, and new analytical solutions are needed in order to estimate more accurately the buckling features in presence of torsion. New experiments accounting for possible torsional effects are required.

- Until now, there is quite few research on the influence of residual stresses on the lateral buckling of submarine pipelines. These effects may be various, depending on the distribution of residual stresses within the pipes. The understanding of the sensitivity of pipelines with respect to residual stresses, regarding the initiation and propagation of lateral buckles, still requires a lot of work.

- Traditional methods for the prediction of pipeline buckling loads, which broadly consist of mathematically solving the stability equations, suffer from large limitations inherent to the natural complexity of the model, and inevitably require strong modeling assumptions so that they can be used. By contrast, data-driven methods (e.g., machine learning) have the natural advantage to not have to cope with too many mathematical issues, from the standpoint of engineering. Therefore, the use of such methods should be generalized for a smart prediction of pipeline buckling in the near future under the context of current digitalization tendency in industry. The extensive data collection from both numerical simulations and experimental tests (or on-site inspections) is the main stumbling block to be figured out in order to fulfill this target.

- With the development of the exploitation of natural sources into ultra-deep water, some innovative types of pipe, such as the PIP pipeline, have been designed. The influential parameters of these new structures on their lateral buckling have not been fully clarified yet. The consequence of the lateral buckling on their structural failure under deep water is not clear as well. Further investigations are also needed to be done.

Acknowledgments

The authors are grateful to the Brittany Regional Council (France) for its financial support (Contract no. SAD18003).

References

Abaqus6.17, 2017. Abaqus: User's Manual, 6.17.

Agusta, A., Ji, G., Sævik, S., 2016. Non-linear clay soil model for lateral pipe-soil interaction. In: ASME 2016 35th International Conference on Ocean, Offshore and Arctic Engineering. American Society of Mechanical Engineers, pp. V005T04A038–V005T04A038.

Allan, T., 1968. One-way buckling of a compressed strip under lateral loading. Journal of Mechanical Engineering Science 10 (2), 175–181.

Alves, L., Sousa, J. R., Ellwanger, G. B., 2012. Transient thermal effects and walking in submarine pipelines. International Journal of Modeling and Simulation for the Petroleum Industry 6 (1).

Amirat, A., Chaoui, K., Azari, Z., Pluvinage, G., 2004. Residual stress analysis in seamless api x60 steel gas pipelines. Sciences & Technologie. B, Sciences de l'ingénieur, 7–10.

Anand, S., Aganwal, S. L., et al., 1980. Field and laboratory studies for evaluating submarine pipeline frictional resistance. In: Offshore Technology Conference. Offshore Technology Conference.

Bai, Q., Bai, Y., 2014a. Subsea pipeline design, analysis, and installation. Gulf Professional Publishing.

Bai, Q., Qi, X., Brunner, M. S., et al., 2009. Global buckle control with dual sleepers in hp/ht pipelines. In: Offshore Technology Conference. Offshore Technology Conference.

Bai, Y., Bai, Q., 2014b. Subsea pipeline integrity and risk management. Gulf Professional Publishing.

Bai, Y., Igland, R., Moan, T., et al., 1993. Tube collapse under combined pressure, tension and bending loads. International Journal of offshore and polar engineering 3 (02).

Bartolini, L. M., Battistini, A., Marchionni, L., Parrella, A., Spinazzè, M., Vitali, L., 2014. Pipe strength and deformation capacity: A novel FE tool for the numerical lab. In: ASME 2014 33rd International Conference on Ocean, Offshore and Arctic Engineering. American Society of Mechanical Engineers, pp. V06BT04A058–V06BT04A058.

Bažant, Z. P., 2000. Structural stability. International Journal of Solids and Structures 37 (1-2), 55–67.

Bishop, C. M., 2006. Pattern recognition and machine learning. springer.

Bjerrum, L., 1973. Geotechnical problems involved in foundations of structures in the north sea. Geotechnique 23 (3), 319–358.

Bjoerhovde, R., 1973. Deterministic and probabilistic approaches to the strength of steel columns.

Brennodden, H., Sveggen, O., Wagner, D., Murff, J., et al., 1986. Full-scale pipe-soil interaction tests. In: Offshore Technology Conference. Offshore Technology Conference.

Bruton, D., Carr, M., Crawford, M., Poiate, E., 2005. The safe design of hot on-bottom pipelines with lateral buckling using the design guideline developed by the safebuck joint industry project. In: Proceedings of the Deep Offshore Technology Conference, Vitoria, Espirito Santo, Brazil.

Bruton, D., White, D., Cheuk, C., Bolton, M., Carr, M., et al., 2006. Pipe/soil interaction behavior during lateral buckling, including large-amplitude cyclic displacement tests by the safebuck jip. In: Offshore Technology Conference. Offshore Technology Conference.

BS8010, 1993. Code of practice for pipelines, part 3: Pipelines subsea: Design, construction and installation. British Standards Institution.

Cai, J., 2018. Residual Ultimate Strength of Seamless Metallic Pipelines with Structural Damage. Delft University of Technology.

Cai, J., Jiang, X., Lodewijks, G., 2017. Residual ultimate strength of offshore metallic pipelines with structural damage–a literature review. Ships and Offshore Structures, 1–19.
URL http://dx.doi.org/ 10.1080/17445302.2017.1308214

Cai, J., Jiang, X., Lodewijks, G., 2018a. Numerical investigation of residual ultimate strength of dented metallic pipes subjected to pure bending. Ships and Offshore Structures.
URL https://doi.org/10.1080/17445302.2018.1430200

Cai, J., Jiang, X., Lodewijks, G., Pei, Z., Wu, W., 2018b. Residual ultimate strength of damaged seamless metallic pipelines with combined dent and metal loss. Marine Structures 61, 188–201.
URL https://doi.org/10.1016/j.marstruc.2018.05.006

Cai, J., Jiang, X., Lodewijks, G., Pei, Z., Wu, W., 2018c. Residual ultimate strength of damaged seamless metallic pipelines with metal loss. Marine Structures 58, 242–253.

Cai, J., Jiang, X., Lodewijks, G., Pei, Z., Wu, W., 2018d. Residual ultimate strength of seamless metallic pipelines - a numerical investigation. Ocean Engineering 164, 148–159.
URL https://doi.org/10.1016/j.oceaneng.2018.06.044

Cai, J., Jiang, X., Lodewijks, G., Pei, Z., Zhu, L., 2019. Experimental investigation of residual ultimate strength of damaged metallic pipelines. Journal of Offshore Mechanics and Arctic Engineering 141 (1), 011703.

Cai, J., Jiang, X., Lodewijks, G., Yang, Y., Wang, M., 2020. Residual ultimate strength of damaged seamless metallic pipelines with combined dent and metal loss. Marine Structures.

Cai, J., You, Y.-x., Li, W., Shi, Z.-m., Qu, Y., 2010. The viv characteristics of deep-sea risers with high aspect ratio in a uniform current profile [j]. Chinese Journal of Hydrodynamics 1.

Chatterjee, S., White, D., Randolph, M., 2012. Numerical simulations of pipe-soil interaction during large lateral movements on clay. Géotechnique 62 (8), 693.

Chee, J., Walker, A., White, D., 2018. Controlling lateral buckling of subsea pipeline with sinusoidal shape pre-deformation. Ocean Engineering 151, 170–190.

Chen, W.-F., Han, D., 1985. Tubular members in offshore structures. Vol. 1. Pitman Publishing.

Chen, W. F., Lui, E. M., 1987. Structural stability: theory and implementation. Tech. rep.

Cheuk, C., Bolton, M., 2006. A technique for modelling the lateral stability of on-bottom pipelines in a small drum centrifuge. In: Proc. Int. Conf. on Physical Modelling in Geotechnics, Hong Kong.

Cheuk, C., White, D., Bolton, M., 2007. Large-scale modelling of soil–pipe interaction during large amplitude cyclic movements of partially embedded pipelines. Canadian Geotechnical Journal 44 (8), 977–996.

Chin, K. T., Arumugam, T., Karuppanan, S., Ovinis, M., 2020. Failure pressure prediction of pipeline with single corrosion defect using artificial neural network. Pipeline Science and Technology 4 (1 (3)), 10–17.

Croll, J. G., 1997. A simplified model of upheaval thermal buckling of subsea pipelines. Thin-Walled Structures 29 (1-4), 59–78.

da Costa, A. M., de Oliveira Cardoso, C., dos Santos Amaral, C., Andueza, A., 2002. Soil-structure interaction of heated pipeline buried in soft clay. In: 2002 4th international pipeline conference. American Society of Mechanical Engineers, pp. 457–466.

De Masi, G., Gentile, M., Vichi, R., Bruschi, R., Gabetta, G., 2015. Machine learning approach to corrosion assessment in subsea pipelines. In: OCEANS 2015-Genova. IEEE, pp. 1–6.

de Oliveira Cardoso, C., Solano, R. F., et al., 2015. Performed of triggers to control thermal buckling of subsea pipelines using reduced scale model. In: The Twenty-fifth International Ocean and Polar Engineering Conference. International Society of Offshore and Polar Engineers.

Dingle, H., White, D., Gaudin, C., 2008. Mechanisms of pipe embedment and lateral breakout on soft clay. Canadian Geotechnical Journal 45 (5), 636–652.

DNV, 2017a. DNVGL-RP-F105 free spanning pipelines. Det Norske Veritas.

DNV, 2017b. DNVGL-RP-F109 on-bottom stability design of submarine pipelines. Det Norske Veritas.

DNV, 2017c. DNVGL-ST-F101 submarine pipeline systems. Det Norske Veritas.

DNV, 2018. DNVGL-RP-F110 global buckling of submarine pipelines. Det Norske Veritas.

Es, S., Gresnigt, A., Vasilikis, D., Karamanos, S., 2016. Ultimate bending capacity of spiral–welded steel tubes–part i: Experiments. Thin-Walled Structures 102, 286–304.

Feng, X., Wu, W., Li, X., Zhang, X., Zhou, J., 2015. Experimental investigations on detecting lateral buckling for

subsea pipelines with distributed fiber optic sensors. Smart Structures and Systems 15 (2), 245–258.
Fukami, K., Fukagata, K., Taira, K., 2020. Assessment of supervised machine learning methods for fluid flows. Theoretical and Computational Fluid Dynamics, 1–23.
Fyrileiv, O., Aamlid, O., Venås, A., Collberg, L., 2013. Deepwater pipelines–status, challenges and future trends. Proceedings of the Institution of Mechanical Engineers, Part M: Journal of Engineering for the Maritime Environment 227 (4), 381–395.
Fyrileiv, O., Collberg, L., 2005. Influence of pressure in pipeline design:effective axial force. In: ASME 2005 24th International Conference on Offshore Mechanics and Arctic Engineering. American Society of Mechanical Engineers, pp. 629–636.
Galambos, T. V., 1998. Guide to stability design criteria for metal structures. John Wiley & Sons.
Galgoul, N. S., Massa, A. L. L., Claro, C. A., 2004. Lateral buckling: Trying to be less conservative. In: 2004 International Pipeline Conference. American Society of Mechanical Engineers, pp. 1899–1904.
Ghaboussi, J., Sidarta, D., 1998. New nested adaptive neural networks (nann) for constitutive modeling. Computers and Geotechnics 22 (1), 29–52.
Gholami, H., Shahrooi, S., Shishesaz, M., 2020. Predicting the burst pressure of high-strength carbon steel pipe with gouge flaws using artificial neural network. Journal of Pipeline Systems Engineering and Practice 11 (4), 04020034.
Guo, B., Song, S., Ghalambor, A., 2013. Offshore pipelines: design, installation, and maintenance. Gulf Professional Publishing.
Haghighat, E., Raissi, M., Moure, A., Gomez, H., Juanes, R., 2020. A deep learning framework for solution and discovery in solid mechanics: linear elasticity. arXiv preprint arXiv:2003.02751.
Harrison, G., Harrison, M., Bruton, D., et al., 2003. King flowlines-thermal expansion design and implementation. In: Offshore Technology Conference. Offshore Technology Conference.
Hobbs, R. E., 1984. In-service buckling of heated pipelines. Journal of Transportation Engineering 110 (2), 175–189.
Hong, Z., Liu, R., Liu, W., Yan, S., 2015a. A lateral global buckling failure envelope for a high temperature and high pressure (ht/hp) submarine pipeline. Applied Ocean Research 51, 117–128.
Hong, Z., Liu, R., Liu, W., Yan, S., 2015b. Study on lateral buckling characteristics of a submarine pipeline with a single arch symmetric initial imperfection. Ocean engineering 108, 21–32.
Hoor, A., Singh, S., Baxter, F., Jesudasen, S., Zeng, W., Simpson, N., Watson, R., Krishnappa, N., et al., 2014. Lateral buckling of pipelines in deepwater gom. In: Offshore Technology Conference. Offshore Technology Conference.
ISO, 2016. Petroleum and natural gas industries–specific requirements for offshore structures–part 4: Geotechnical and foundation design considerations. 19901-4: 2016.
Jayson, D., Delaporte, P., Albert, J., Prevost, M., Bruton, D., Sinclair, F., 2008. Greater plutonio project–subsea flowline design and performance. In: Offshore Pipeline Technology Conference.
Jr, J. S., Shadley, J., Rybicki, E., 1990. Experimental method for determining through thickness residual hoop stresses in thin walled pipes and tubes without inside access. Strain 26 (1), 7–14.
Ju, G., Kyriakides, S., 1988. Thermal buckling of offshore pipelines. Journal of Offshore Mechanics and Arctic Engineering 110 (4), 355–364.
Jukes, P., Eltaher, A., Sun, J., Harrison, G., 2009. Extra high-pressure high-temperature (xhpht) flowlines: Design considerations and challenges. In: ASME 2009 28th International Conference on Ocean, Offshore and Arctic Engineering. American Society of Mechanical Engineers, pp. 469–478.
Karal, K., et al., 1977. Lateral· stability of submarine pipelines. In: Offshore Technology Conference. Offshore Technology Conference.
Karampour, H., 2018. Effect of proximity of imperfections on buckle interaction in deep subsea pipelines. Marine Structures 59, 444–457.
Karampour, H., Albermani, F., 2014. Experimental and numerical investigations of buckle interaction in subsea pipelines. Engineering Structures 66, 81–88.
Karampour, H., Albermani, F., Gross, J., 2013a. On lateral and upheaval buckling or subsea pipelines. Engineering structures 52, 317–330.
Karampour, H., Albermani, F., Veidt, M., 2013b. Buckle interaction in deep subsea pipelines. Thin-Walled Structures 72, 113–120.
Kerr, A. D., 1978. Analysis of thermal track buckling in the lateral plane. Acta Mechanica 30 (1-2), 17–50.

Konuk, I., 2018. Coupled lateral and axial soil-pipe interaction and lateral buckling part ii: Solutions. International Journal of Solids and Structures 132, 127–152.

Konuk, I., Yu, S., 2007. Continuum fe modeling of lateral buckling: study of soil effects. In: ASME 2007 26th International Conference on Offshore Mechanics and Arctic Engineering. American Society of Mechanical Engineers, pp. 347–354.

Lambrakos, K., 1985. Marine pipeline soil friction coefficients from in-situ testing. Ocean engineering 12 (2), 131–150.

Le Grognec, P., Nême, A., Cai, J., 2020. Investigation of the torsional effects on the lateral buckling of a pipe-like beam resting on the ground under axial compression. International Journal of Structural Stability and Dynamics 20 (9), 2050110.

LeCun, Y., Bengio, Y., Hinton, G., 2015. Deep learning. nature 521 (7553), 436–444.

Liu, R., Basu, P., Xiong, H., 2015. Laboratory tests and thermal buckling analysis for pipes buried in bohai soft clay. Marine Structures 43, 44–60.

Liu, R., Wang, X., 2018. Lateral global buckling high-order mode analysis of a submarine pipeline with imperfection. Applied Ocean Research 73, 107–126.

Liu, R., Xiong, H., Wu, X., Yan, S., 2014. Numerical studies on global buckling of subsea pipelines. Ocean Engineering 78, 62–72.

Liu, Y., 2013. Overview of submarine pipeline global buckling. In: 2013 Fourth International Conference on Digital Manufacturing & Automation. IEEE, pp. 903–906.

Lynch, J., 1952. The measurement of residual stresses. American Society for Metals, Residual Stress Measurements, Cleveland, OH, 42–96.

Lyons, C., et al., 1973. Soil resistance to lateral sliding of marine pipelines. In: Offshore Technology Conference. Offshore Technology Conference.

Maltby, T. C., Calladine, C. R., 1995a. An investigation into upheaval buckling of buried pipelines—i. experimental apparatus and some observations. International journal of mechanical sciences 37 (9), 943–963.

Maltby, T. C., Calladine, C. R., 1995b. An investigation into upheaval buckling of buried pipelines—ii. theory and analysis of experimental observations. International journal of mechanical sciences 37 (9), 965–983.

Marshall, P. W., 2013. Design of welded tubular connections: basis and use of AWS code provisions. Vol. 37. Elsevier.

McCarron, W., 2015a. Limit analysis and finite element evaluation of lateral pipe–soil interaction resistance. Canadian geotechnical journal 53 (1), 14–21.

McCarron, W., 2015b. Subsea flowline buckle capacity considering uncertainty in pipe-soil interaction. Computers and Geotechnics 68, 17–27.

McCarron, W., 2017. Limit analysis method for evaluating soil resistance to lateral motions of pipelines partially embedded in a seafloor. International Journal of Geomechanics 17 (9), 04017066.

McCarron, W., 2018. Exploring the design space governing the lateral buckle capacity of subsea pipelines. Journal of Pipeline Systems Engineering and Practice 10 (1), 04018033.

McKinnon, C., Mansour, M., Gibbons, N., 2001. Erskine replacement pipeline project–design challenges. In: Proceedings of the 24th Offshore Pipeline Technology Conference, Amsterdam. pp. 26–27.

Miles, D., Calladine, C., 1999. Lateral thermal buckling of pipelines on the sea bed. Journal of applied mechanics 66 (4), 891–897.

Murff, J., Wagner, D., Randolph, M., 1989. Pipe penetration in cohesive soil. Géotechnique 39 (2), 213–229.

Najjar, S., Gilbert, R., Liedtke, E., McCarron, B., Young, A., 2007. Residual shear strength for interfaces between pipelines and clays at low effective normal stresses. Journal of geotechnical and geoenvironmental engineering 133 (6), 695–706.

Nazari, A., Rajeev, P., Sanjayan, J. G., 2015. Modelling of upheaval buckling of offshore pipeline buried in clay soil using genetic programming. Engineering Structures 101, 306–317.

Oliveira, J. R., Almeida, M. S., Almeida, M. C., Borges, R. G., 2010. Physical modeling of lateral clay-pipe interaction. Journal of Geotechnical and Geoenvironmental Engineering 136 (7), 950–956.

Ossai, C. I., 2020. Corrosion defect modelling of aged pipelines with a feed-forward multi-layer neural network for leak and burst failure estimation. Engineering Failure Analysis 110, 104397.

Palmer, A., Baldry, J., et al., 1974. Lateral buckling of axially constrained pipelines. Journal of Petroleum Technology

26 (11), 1–283.
Palmer, A., Ellinas, C., Richards, D., Guijt, J., et al., 1990. Design of submarine pipelines against upheaval buckling. In: Offshore Technology Conference. Offshore Technology Conference.
Palmer, A., Tebboth, L., Miles, D., Calladine, C., 1999. Instability of pipelines on slopes. Journal of applied mechanics 66 (3), 794–799.
Pankhurst, R. C., 1964. Dimensional analysis and scale factors. Taylor & Francis.
Pasqualino, I., Alves, J., Battista, R., 2001. Failure simulation of a buried pipeline under thermal loading. In: Proceedings of the 20th International Conference on Offshore Mechanics and Arctic Engineering (OMAE), Rio De Janiro, Brazil. pp. 3–8.
Peek, R., Yun, H., 2007. Flotation to trigger lateral buckles in pipelines on a flat seabed. Journal of engineering mechanics 133 (4), 442–451.
Perinet, D., Simon, J., et al., 2011. Lateral buckling and pipeline walking mitigation in deep water. In: Offshore Technology Conference. Offshore Technology Conference.
Pirling, T., Carradò, A., Palkowski, H., 2011. Residual stress distribution in seamless tubes determined experimentally and by fem. Procedia Engineering 10, 3080–3085.
Richards, D., 1990. The effect of imperfection shape on upheaval buckling behaviour. In: Advances in subsea pipeline engineering and technology. Springer, pp. 51–66.
Riks, E., 1972. The application of Newton's method to the problem of elastic stability. Journal of Applied Mechanics 39 (4), 1060–1065.
Riks, E., 1979. An incremental approach to the solution of snapping and buckling problems. International Journal of Solids and Structures 15 (7), 529–551.
Safebuck, J., 2008. Safe design of pipelines with lateral buckling, design guideline. Boreas Report No. BR02050/SAFEBUCK/C.
Schotman, G., Stork, F., et al., 1987. Pipe-soil interaction: a model for laterally loaded pipelines in clay. In: Offshore Technology Conference. Offshore Technology Conference.
Sen, D., Aghazadeh, A., Mousavi, A., Nagarajaiah, S., Baraniuk, R., Dabak, A., 2019. Data-driven semi-supervised and supervised learning algorithms for health monitoring of pipes. Mechanical Systems and Signal Processing 131, 524–537.
Shi, R., Wang, L., 2014. Single buoyancy load to trigger lateral buckles in pipelines on a soft seabed. Journal of Engineering Mechanics 141 (5), 04014151.
Sinclair, F., Carr, M., Bruton, D., Farrant, T., 2009. Design challenges and experience with controlled lateral buckle initiation methods. In: ASME 2009 28th International Conference on Ocean, Offshore and Arctic Engineering. American Society of Mechanical Engineers, pp. 319–330.
Song, C., Teng, J., Rotter, J., 2004. Imperfection sensitivity of thin elastic cylindrical shells subject to partial axial compression. International Journal of Solids and Structures 41 (24), 7155–7180.
Sonin, A. A., 2001. The physical basis of dimensional analysis. Department of Mechanical Engineering, MIT, Cambridge, MA, 1–57.
Sotberg, T., Verley, R., 1992. A soil resistance model for pipelines on sandy soils. OMAE, Vols. VA, Pipeline Technology, 123–131.
Taylor, N., Gan, A. B., 1986. Submarine pipeline buckling—imperfection studies. Thin-Walled Structures 4 (4), 295–323.
Taylor, N., Richardson, D., Gan, A., 1985. On submarine pipeline frictional characteristics in the presence of buckling. In: Proceedings of the 4th International Offshore Mechanics and Arctic Engineering Symposium. Vol. 1. pp. 508–515.
Taylor, N., Tran, V., 1993. Prop-imperfection subsea pipeline buckling. Marine structures 6 (4), 325–358.
Taylor, N., Tran, V., 1996. Experimental and theoretical studies in subsea pipeline buckling. Marine Structures 9 (2), 211–257.
Timoshenko, S., Gere, J., 2009. Theory of elastic stability. Courier Corporation.
Toma, S., Chen, W. F., 1979. Analysis of fabricated tubular columns. Journal of the Structural Division 105 (11), 2343–2366.
Traub, J. F., 1982. Iterative methods for the solution of equations. Vol. 312. American Mathematical Soc.

Urthaler, Y., Watson, R., Davis, J., 2012. Lateral buckling of deepwater pipelines in operation. In: ASME 2012 31st International Conference on Ocean, Offshore and Arctic Engineering. American Society of Mechanical Engineers, pp. 783–792.

Van den Abeele, F., Boël, F., Hayes, D., Scales, D., 2015. An integrated numerical approach to design offshore pipelines susceptible to lateral buckling. In: ASME 2015 34th International Conference on Ocean, Offshore and Arctic Engineering. American Society of Mechanical Engineers, pp. V05AT04A023–V05AT04A023.

Vasilikis, D., Karamanos, S., Es, S., Gresnigt, A., 2015. Ultimate bending capacity of spiral–welded steel tubes–part ii:predictions. Thin-Walled Structures.

Vedeld, K., Sollund, H., Hellesland, J., Fyrileiv, O., 2014. Effective axial forces in offshore lined and clad pipes. Engineering Structures 66, 66–80.

Verley, R., Lund, K., 1995. A soil resistance model for pipelines placed on clay soils. In: ASME 1995 14th International Conference on Offshore Mechanics and Arctic Engineering. Vol. 5. American Society of Mechanical Engineers, pp. 225–232.

Verley, R., Sotberg, T., 1994. A soil resistance model for pipelines placed on sandy soils. Journal of Offshore Mechanics and Arctic Engineering 116 (3), 145–153.

Wagner, D. A., Murff, J. D., Brennodden, H., Sveggen, O., 1989. Pipe-soil interaction model. Journal of Waterway, Port, Coastal, and Ocean Engineering 115 (2), 205–220.

Wang, Y., Liu, R., Wang, L., 2018a. Experimental and upper-bound analysis of lateral soil resistance for shallow-embedded pipeline in bohai sand. Journal of Pipeline Systems Engineering and Practice 9 (4), 04018014.

Wang, Z., Chen, Z., Liu, H., Zhang, Z., 2017. Numerical study on lateral buckling of pipelines with imperfection and sleeper. Applied Ocean Research 68, 103–113.

Wang, Z., Tang, Y., van der Heijden, G., 2018b. Analytical study of distributed buoyancy sections to control lateral thermal buckling of subsea pipelines. Marine Structures 58, 199–222.

Wang, Z., Tang, Y., van der Heijden, G., 2018c. Analytical study of lateral thermal buckling for subsea pipelines with sleeper. Thin-Walled Structures 122, 17–29.

Wang, Z., van der Heijden, G., , Tang, Y., 2018d. Analytical study of third-mode lateral thermal buckling for unburied subsea pipelines with sleeper. Engineering Structures 168, 447–461.

White, D., Cheuk, C., 2008. Modelling the soil resistance on seabed pipelines during large cycles of lateral movement. Marine structures 21 (1), 59–79.

Xie, M., Tian, Z., 2018. A review on pipeline integrity management utilizing in-line inspection data. Engineering Failure Analysis 92, 222–239.

Young, W. C., Budynas, R. G., Sadegh, A. M., et al., 2002. Roark's formulas for stress and strain. Vol. 7. McGraw-Hill New York.

Zeng, X., Duan, M., 2014. Mode localization in lateral buckling of partially embedded submarine pipelines. International Journal of Solids and Structures 51 (10), 1991–1999.

Zeng, X., Duan, M., Che, X., 2014. Critical upheaval buckling forces of imperfect pipelines. Applied Ocean Research 45, 33–39.

Zhang, J., Stewart, D., Randolph, M., 2002. Kinematic hardening model for pipeline-soil interaction under various loading conditions. The International Journal of Geomechanics 2 (4), 419–446.

Zhang, X., Duan, M., 2015. Prediction of the upheaval buckling critical force for imperfect submarine pipelines. Ocean Engineering 109, 330–343.

Zhang, X., Duan, M., Soares, C. G., 2018a. Lateral buckling critical force for submarine pipe-in-pipe pipelines. Applied Ocean Research 78, 99–109.

Zhang, X., Soares, C. G., An, C., Duan, M., 2018b. An unified formula for the critical force of lateral buckling of imperfect submarine pipelines. Ocean Engineering 166, 324–335.

Zhang, Z., Liu, H., Chen, Z., 2019. Lateral buckling theory and experimental study on pipe-in-pipe structure. Metals 9 (2), 185.

Zhu, J., Attard, M. M., Kellermann, D. C., 2015. In-plane nonlinear localised lateral buckling of straight pipelines. Engineering Structures 103, 37–52.